Clean Growth[*]

Costas Arkolakis

Yale University

Conor Walsh

Columbia University

September 2022 (First Draft, Preliminary)

Abstract

We provide a spatial theory of clean growth to assess the global impact of the rise of renewable energy. We model the details of the combined production and transmission network of electricity ("the grid") that determine the supply and losses of energy in space. Demand is determined through a model of trade and production, and electricity prices are set by regional grid operators. The local rate of clean energy adoption depends on learning-by-doing, the global electricity and trade network, and regional comparative advantage in renewable resources. To quantify the contribution of renewable adoption to global growth, we collect and harmonize global data on transmission lines, power stations, trade, and regional output. We use the model to measure the aggregate and spatial implications of decarbonizing power production, as well as the role of policy in affecting the transition.

---

1   Introduction

The arrival of cheap renewable technologies is bound to substantially change global energy use, power production, and trade. Beginning from virtually zero in the mid 2000's, the share of global electricity produced by new solar and wind technologies has begun to rise rapidly (see left panel of Figure 1). This trend is likely to continue, as capital costs have tended to fall rapidly with overall capacity installation (the right panel of the same Figure), a trend the literature has attributed to technical progress and "learning by doing".[1]

To assess the macroeconomic impact of the rise of renewable resources, we build a new theory of clean growth, embedding the details of the combined production and transmission of electricity ("the grid") in a spatial growth model. In doing so, we construct a dynamic theory of production and transmission of electricity in space, taking into account the physical properties of the electricity network and the losses incurred by transferring electricity from power assets to where it is used.

We start in Section 2 by modeling the details of the electricity production network. Electrical power can be generated from fossil or renewable assets in each region. We use the physical properties of the electrical grid to develop a model of transmission and losses of electricity in space, and analyze the net supply of electricity of each region. The demand for electricity is determined by a multi-sector Armington trade model as in Armington (1969); Anderson (1979). Prices of electricity are set for a set of regions by a local utility planer depending on the supply and demand of electricity in each node.

We then embed this setup in a model of investment in renewable assets. Solar and wind power assets that differ from fossil fuel power capital in four key respects. First, they produce no CO_2 emissions. Second, their electricity output is variable over both daily and seasonal horizons. Third, the productivity of these assets differs markedly across space. Fourth, their production appears subject to continuing cost falls as output of these assets increases. The first two characteristics have received substantial attention in both the literature and popular discussions of the climate crisis. The third and fourth are comparatively less discussed. Nevertheless, they are key to understanding the role of these new technologies in future productivity growth, and are central features of the model we present.

---

[1]See, for example, McDonald and Schrattenholzer (2001) ,Van Benthem et al. (2008) and Rubin et al. (2015).

In Section 3, we provide a novel theory of clean growth driven by technical progress in renewable capital. Local investment in renewable technology depends on local electricity prices now and in the future. The speed of adoption in a given location is determined by the spatial productivity of the renewable capital, which depends on local renewable potential, local economic conditions, and the structure of the electricity grid. As more renewable capital is installed globally, investment prices fall continuously due to global spillovers from learning by doing. This pushes down wholesale power prices on the electricity network, and drives increases in output.

In Section 4, to quantitatively assess the uptake of renewable energy we complement the theory with several newly constructed datasets, harmonized at the regional level. We use a comprehensive database of the world's power plants to measure the current installed non-renewable energy capacity. We incorporate information on renewable potential at a very fine spatial disaggregation for solar and wind technologies. We also construct a comprehensive database on the global electricity networks and their connections. Combining these sources allow us to measure the current capacity of fossil assets and the comparative advantage of different regions in renewable energy. To measure the comparative advantage of regions in 10 major economic sectors, we complement these data with regional data on trade, employment, and output, which we use to estimate bilateral trade costs and productivities. This energy and production potential ultimately determines the uptake of solar and wind renewable energy resources across different regions.

Finally, we use our quantitative model to trace the implications of clean growth for sectoral specialization and total factor productivity across the globe. We find that, in our baseline case with no subsidies, renewables quickly dominate the electric grid, rising to 80% of world power output by 2040. Their adoption leads to dramatic falls in power prices, which fall on average by 76% across the globe. The subsequent increase in industrial output raises real wages by an average of 6%, though with substantial heterogeneity across the globe.

Lastly, we consider the role of policy in shaping the transition. In particular, we model the effects of the Inflation Reduction Act (IRA) passed by the Biden administration in 2030. Among other things, this included a substantial production tax credit for renewable energy in the US. We find that the IRA significantly hastens the adoption of renewable energy in the US, and has modest globel spillovers, driving capital prices lower and increasing adoption in other countries. However, the cost is substantial, and

Figure 1: Progress in Clean Energy
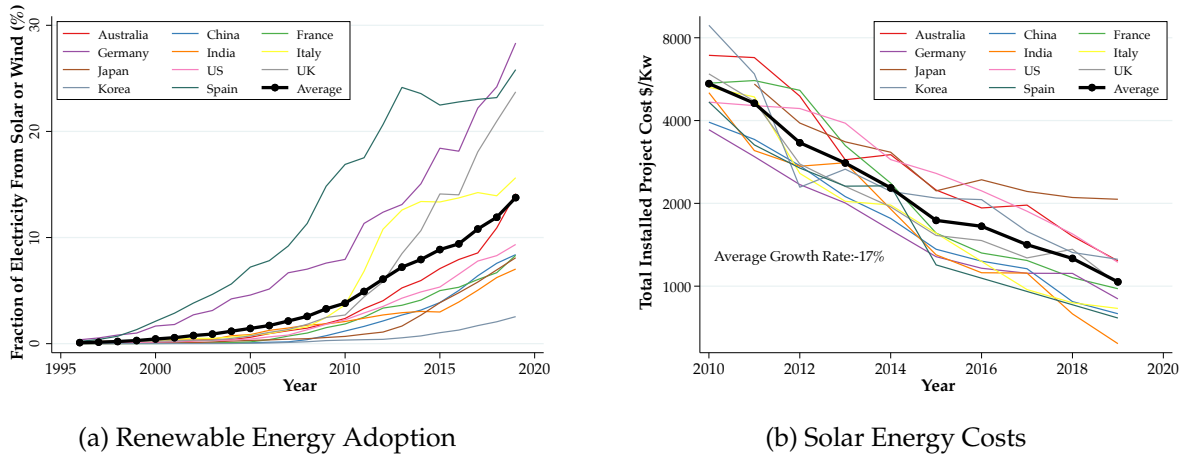
(a) Renewable Energy Adoption   (b) Solar Energy Costs

Notes: The left panel plots the share of a country's total electricity usage that comes from wind or solar. The right panel plots the levelized cost of energy from a new solar energy project across countries.Data for the left panel comes from the International Renewable Energy Agency, while the right panel uses data from the BP Statistical Review.

much of the subsidy goes to inframarginal investment, which would have been installed in the absence of the IRA.

Related Literature. Our work relates to the recent developments in the quantitative spatial and trade literature (see Redding and Rossi-Hansberg, 2017 and Costinot and Rodríguez-Clare, 2014 for in-depth reviews). We show how to use such setups to incorporate supply and demand of energy by explicitly incorporating the electricity grid and renewable or traditional power assets. An interesting feature of our setup is that given electricity prices, determined by the grid, it retains several of the properties of spatial models and allows for the use of the standard techniques of solving for the equilibrium and model counterfactuals. Likewise, we show how to model investment dynamics in a multi-region, multi-sector setup by exploiting the modularity of renewable investment and assuming free entry into renewable investment (Walsh (2021)).

We also contribute to the literature analyzing economic growth and the growth of the renewables sector. As pointed out by Stern (2019) "the core mainstream economic growth models disregard energy or other resources". There are however some recent advances in economic growth that incorporate energy usage in growth models. For example, Tahvonen and Salo (2001) and Fröling (2011) provide a theoretical analysis of the use of renewable energy in a unified growth framework. These works ignore spatial considerations and view renewable technologies as an exogenous cost function, with no

decision of accumulation over time, a consideration obviously relevant for resources such as solar panels, wind farms etc. Golosov et al. (2014) consider optimal taxation of fossil fuels and Kortum and Weisbach (2021); Krusell and Smith Jr (2022) policies taxing CO2 emmisions. Alvarez and Rossi-Hansberg (2021) model the implications of climate change for economic allocations across space with the presence of an energy sector (see also Conte et al. (2021)) .[2] Lastly, due to the challenges involved in modelling the energy transition at a global level, we abstract from many key features of the microeconomics of energy markets and renewable integration; see Wolak (2021) and Tangerås and Wolak (2019).

2   Setup

We consider an electrical grid with J nodes where economic activity and production of electricity takes place. Each node could be the location of an electricity generator, a location where other economic activity takes place and consumes power, or both. We use bold notation to denote vectors and bold with a bar to denote matrices. We start with the description of the electrical grid, the production of electricity, the associated electricity losses, and the power planning problem that determines electricity prices in each region. Subsequently, we embed this setup in a standard spatial economy setup.

2.1   The Electrical Grid

Each node, has a cost of of generation $M_j(Y_j^{\mathcal{E}})$, where $Y_j^{\mathcal{E}}$ is power produced in node $j \in J$. The maximum output of node j is denoted by $\bar{Y}_j^{max}$. Each location has demand for power $D_j(p_j)$ dictated by trade, aggregate demand and supply of labor, which will be determined by our spatial equilibrium setup.[3] We denote by $\boldsymbol{P}$ the vector of dimension $(J-1)$ and its element P_j to be the net power output of node j, such that

$$P_j = Y_j^{\mathcal{E}} - D_j. \tag{1}$$

---

[2]At the same time, energy usage has been recently the topic of work in industrial organization (see, for example, Asker et al., 2019, Hodgson, 2019).

[3]We assume that the demand for energy is continuously differentiable and decreasing in p_j, and diverges as $p_j \to 0$ We show that these assumptions hold from the energy demand function resulting from the quantitative trade model of Section 2.5.

We will clarify below how the power in Jth node (also called the *swing bus*) is determined.

The electrical grid also consists of power lines that connect a subset of the power nodes. This grid is represented by a matrix $\bar{A}$ of dimension $K \times (J-1)$, with an entry of 1 or -1 in the (k, j) cell if node j is connected to line k and where K is the number of lines. We consider only bilateral links. Power flows on all lines are represented by the vector $\mathbf{Z}$ with element Z_{jk}. Flows can take on positive or negative values; if Z_{jk} is positive it indicates power flowing from node j through line k. Each line also has a maximum amount of power that can flow on it, the *transmission capacity*, which we denote as $\bar{Z}_k^{max}$, such that $|Z_k| \leq \bar{Z}_k^{max}$. Lastly, each line has a resistance R_k and an inductance X_k. Both are determined by physical properties of the line, including the line length and materials: Resistance measures how strongly a line resists electrical current flowing through it, while inductance is relevant for AC power networks and measures how strongly a line resists changes in electrical current.

2.2 Electricity Production

Electricity production in a node depends on the amount of power capital installed in that node. Capital in a node j is owned by the agents who live in the region j. Power capital comes in two types: renewable ($\mathcal{R}$) and fossil fuel ($\mathcal{F}$), with amounts $K_j^{\mathcal{R}}$ and $K_j^{\mathcal{F}}$, respectively. Renewable capital produces

$$Y_j^{\mathcal{R}} = \theta_j K_j^{\mathcal{R}} \tag{2}$$

units of electricity per period, where θ_j is a local renewable potential. That is, renewable capital produces power with no inputs, and at zero marginal cost.

Fossil fuel capital instead requires the use of fossil fuel inputs, the total use of which in j is denoted F_j, and total electricity produced from fossil fuels is

$$Y_j^{\mathcal{F}} = f(K_j^{\mathcal{F}}, F_j)$$

where f is continuous and strictly increasing in each of its arguments, and for fixed capital $K_j^{\mathcal{F}}$ is concave in F_j.

5

Figure 2: Global Renewable Potential

(a) Solar Potential
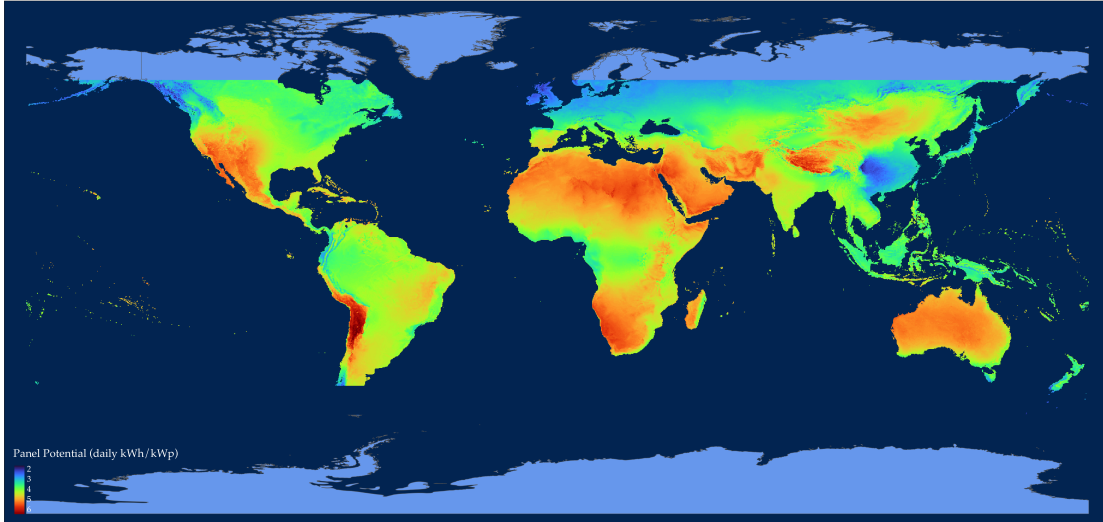
(b) Wind Potential
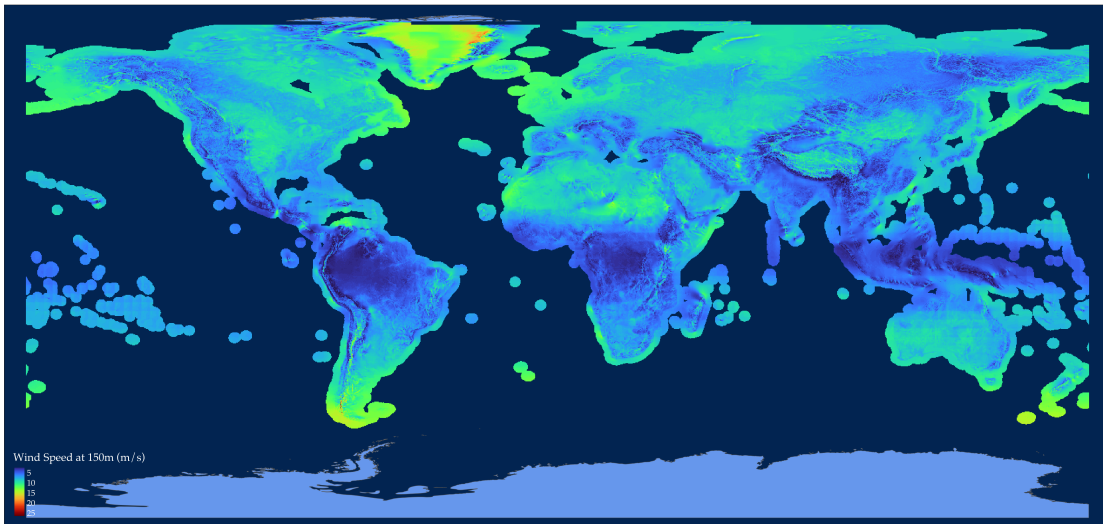
Notes: Panel (A) shows solar panel potential (defined as daily kWh per peak kilowatt rating of the panel) using data from the Global Solar Atlas. Panel (B) shows wind electricity potential (average daily wind speeds) using data from the Global Wind Atlas.

We denote the total electricity production as $Y_j^{\mathcal{E}}$ so that

$$Y_j^{\mathcal{E}} = Y_j^{\mathcal{R}} + Y_j^{\mathcal{F}}. \tag{3}$$

Fossil fuel is available for a fixed price of $p^{\mathcal{F}}$ in units of a final numeraire good (specified below), and can be bought anywhere for the same price. The total cost of producing power $Y_j^{\mathcal{E}}$ is (abusing notation slightly)

$$M_j(Y_j^{\mathcal{E}}) = \begin{cases} p^{\mathcal{F}} \left(f^{K_j^{\mathcal{F}}} \right)^{-1} (Y_j^{\mathcal{E}} - \theta_j K_j^{\mathcal{R}}) & \text{if } Y_j^{\mathcal{E}} > \theta_j K_j^{\mathcal{R}} \\ 0 & \text{if } Y_j^{\mathcal{E}} \leq \theta_j K_j^{\mathcal{R}} \end{cases}$$

where $\left(f^{K_j^{\mathcal{F}}} \right)^{-1}$ denotes the inverse function of f when fossil capital is held fixed at K. This formulation reflects the process of "merit order dispatch" common to power networks: the lowest marginal cost power stations are dispatched to supply the grid (the operation of which is described below), and then power is scheduled in order of increasing marginal cost. We also assume that renewable capital does not need to be operated at full capacity, but can have its power output scaled up or down as required with no cost. Lastly, there is a maximum fossil fuel input F_j^{max}, such that maximum power production in a node is

$$\bar{Y}_j^{max} = \theta_j K_j^{\mathcal{R}} + f(K_j^{\mathcal{F}}, F_j^{max})$$

Assuming we know the power generated in each power node and the grid we can determine the losses given the power flows. We do that next.

2.3 Electricity Losses

The distribution of electric power across the grid incurs losses. However, flows cannot be allocated to a line. They are determined from Kirkhoff's laws and the amount of generation and consumption in each node. In addition, the power system must at all times satisfy the energy balance constraint

$$\sum_j D_j + \lambda = \sum_j Y_j^{\mathcal{E}} \tag{4}$$

so that total energy used, plus total systems losses λ, is equal to that produced across all power assets.

Based on these properties of the grid and the power flow, we can approximate the loss in each line in the grid as $\lambda_k = R_k Z_k^2$, as we show in Appendix A3. The total transmission loss function is a function of all of these flows, denoted $\lambda(\mathbf{Z})$. Therefore, the overall loss can be written as

$$\lambda(\mathbf{Z}) = \sum_k R_k Z_k^2. \tag{5}$$

Our next aim is to derive the total loss on the network as a function of net power in each node j and the transmission network features. In the appendix, we show that the relationship between power in each line and the power nodes can be written as

$$\mathbf{Z} = \bar{\mathbf{\Omega}} \bar{\mathbf{A}} (\bar{\mathbf{A}}' \bar{\mathbf{\Omega}} \bar{\mathbf{A}})^{-1} \mathbf{P} \tag{6}$$

where $\bar{\mathbf{\Omega}}$ is a $K \times K$ diagonal matrix of "line admittances" such that $\Omega_k = (R_k^2 + X_k^2)^{-\frac{1}{2}}$ (i.e. its elements are inversely related to resistance R_k and inductance X_k).

Now since line losses are given by (5) we can express losses in terms of the characteristics of the network and the power generated by each asset according to the following lemma:

Lemma 1. *Power losses in the system can be expressed in a quadratic form:*

$$\lambda = \mathbf{P}' \bar{\mathbf{B}} \mathbf{P} \tag{7}$$

where

$$\bar{\mathbf{B}} = (\bar{\mathbf{A}}' \bar{\mathbf{R}}^{-1} \bar{\mathbf{A}})^{-1} \tag{8}$$

is a positive semi-definite $(J-1) \times (J-1)$ matrix of fundamentals and $\bar{\mathbf{R}}$ is a $K \times K$ diagonal matrix of line resistances.

This representation of losses — its elegance notwithstanding — is useful for two purposes. First, it allows to express the relation between losses in the network and power generation across nodes in terms of the measurable features of the network summarized in the matrix $\bar{\mathbf{B}}$ in equation (8) uses information for the power network links and their associated resistances. Given the net output power of each node, this information is

a sufficient statistic for the losses in each line. Second, the fact that $\bar{B}$ is positive semi-definite is important in allowing us to characterize the problem of the power network planning problem.

2.3.1 Examples

We provide two examples of electricity networks for illustration using stylized network structures. These are the symmetric star network, with the swing bus in the center and connecting on single lines to demand nodes, and an analogous ring network. In these cases, the network incidence matrices are given by

$$
\bar{A}_{star} = \begin{bmatrix} 1 & 0 & 0 & 0 & 0 \\ 0 & 1 & 0 & 0 & 0 \\ 0 & 0 & 1 & 0 & 0 \\ 0 & 0 & 0 & 1 & 0 \\ 0 & 0 & 0 & 0 & 1 \end{bmatrix} \qquad
\bar{A}_{ring} = \begin{bmatrix} 1 & 0 & 0 & 0 \\ -1 & 1 & 0 & 0 \\ 0 & -1 & 1 & 0 \\ 0 & 0 & -1 & 1 \\ 0 & 0 & 0 & -1 \end{bmatrix}
$$

See Figure A4 for a visual representation of these two stylized network structures, with the swing bus in blue. These examples are used to illustrate the theory below.

2.4 The Power Network Planning Problem

We assume the presence of a centralized power network administrator over a collection of connected nodes j that aims to maximize economy wide output net of generation costs by setting local electricity prices. For example, in the continental United States the power grid is made up of three main interconnected transmission networks: the Eastern Interconnection encompasses the area east of the Rocky Mountains and a portion of the Texas panhandle, the Western Interconnection encompasses the area to the west of the Rocky Mountains and the Electric Reliability Council of Texas (ERCOT) that covers most of Texas. While there are minimal connections between these three transmission networks, and to the foreign networks in Canada and Mexico, the power capacity of these connections is very small and we treat these networks as independent. Thus, the power grid mechanics described above will hold for each of these networks separately.

Figure 3: The United States Transmission Grid

VOLTAGE

— 0 to 200
— 200 to 400
— 400 to 600
— 600 to 800
— 800 to 1,000
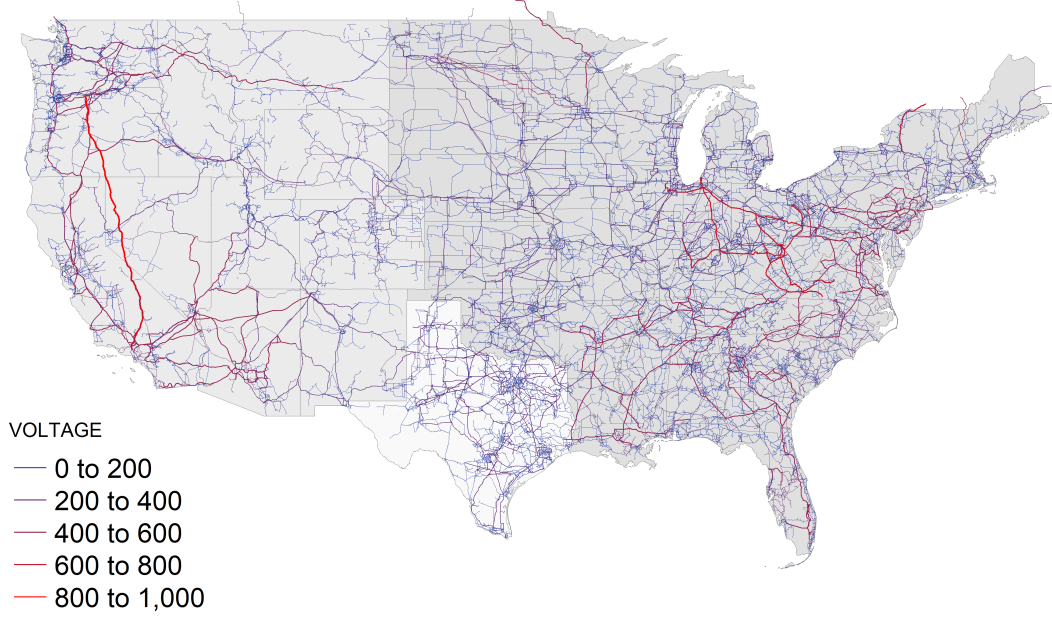
Notes: This Figure shows the high voltage transmission network of the United States as well as the interconnections between the networks using data from the U.S. Energy Information Administration. While there are a few small interconnections between the three networks, they are effectively independent.

In Figure 3 we depict the entire continental United States network, and the areas covered by the three power transmission networks are shaded with a different grey.

We assume that the network administrators have an objective that maximizes the total production of their network. Let $Q_j(D_j)$ be a total local domestic product in region j, which is strictly increasing in power usage D_j. As above, M_j is the cost of generating energy output $Y_j^{\mathcal{E}}$ in node j, in units of the final good. We assume here the existence of a continuously differentiable, non-increasing demand function $D_i(p_i^{\mathcal{E}})$ at the regional level for power in the price of electricity $p_j^{\mathcal{E}}$. The particular details of this function which arise from a model of trade across space are presented below in Section 2.5. A continuous differentiable, non-decreasing supply function $Y^{\mathcal{E}}(p_j^{\mathcal{E}})$ is also derived. The problem of the administrator is to choose prices $\{p_j^{\mathcal{E}}\}$ in the lines that it administers in order to solve

$$\max_{\{p_j^{\mathcal{E}}\}} \sum_j p_j Q_j(D_j(p_j^{\mathcal{E}})) - \sum_j M_j(Y_j^{\mathcal{E}}(p_j^{\mathcal{E}})) \tag{9}$$

subject to the net power production in each power node equation (1), the energy balance constraint in equation (4), equation (7) that determines the losses in the network, the power in each link equation (6), and the network constraint for each link, $Z_k \leq \bar{Z}_k^{max}$. Importantly, we assume that the grid administrator takes the output price p_j as given.

Proposition 1. *If Q_j is strictly concave for all j, then the planner's problem has a unique solution, and can be implemented by setting spatial prices in each node i according to*

$$p_j^{\mathcal{E}} = \mu + \mu \frac{\partial \lambda}{\partial D_j} + \sum_k \eta_k \frac{\partial Z_k}{\partial D_j}$$

where η_k is the shadow value of extra capacity on a constrained line k, and μ is the shadow value of total generation capacity.

The price of electricity in any node thus consists of three intuitive components. First, μ, is the shadow value of total generation capacity, determined by the last unit of electricity generation used by the grid. Second, is the marginal impact of the losses of demanding more (net) power in a location. The last term is determined by the overall line capacity constraints.

We assume that any profits or losses of the electricity network are rebated uniformly to the consumers that correspond to the administrative boundaries of each transmission network. While it is simple to show that the price of electricity is always higher in nodes that are net users of power, it does not follow that the electricity network always makes a positive profit since they must absorb transmission losses. The profits from the operation of the electricity network in a region j belonging to the transmission network $\mathcal{T}$ are denoted by

$$\Pi_j^{\mathcal{T}} = \sum_i \left(p_i^{\mathcal{E}} D_i - p^{\mathcal{E}} Y_i^{\mathcal{E}} \right) \frac{L_j}{\sum_i L_i}$$

where L_j is population of region j.

Intermittency. So far we have ignored the intermittency of electricity production of renewable capital, which is a central issue in the uptake of this technology. The output of fossil fuel capital is largely predictable and can be scheduled and controlled in advance (severe weather events such as the Texas blackout of 2021 notwithstanding). This is not so true for solar and wind energy sources.

11

There are two dimensions to this intermittency. First, there is a strong seasonal component to electricity produced from renewable electricity (Mulder, 2014). On the one hand, outside of the equator, solar capital produces significantly less electricity in the winter. On the other hand, wind speeds tend to be higher in the winter in many places in the globe for wind turbines. Within the model, this can be handled in a natural way, by defining the period t to occur at the sub-year level, and allowing the renewable potential θ_{jt} to depend on calendar time t. We pursue this extension in the quantitative analysis.

Second, renewable electricity production has marked variation on a daily time scale, fluctuating substantially from day to day for both wind and solar capital (depending on wind speeds and cloud cover/night respectively). Due to the complexity of doing so at a world scale, we avoid modeling the stochastic scheduling problem of each utility directly, which involves setting variable wholesale prices across different periods of the day in response to both predicted and observed weather patterns. This variation in daily prices provides substantial opportunities for battery arbitrage as battery prices continue to fall (Nykvist and Nilsson, 2015). While stand-alone merchant batteries are beginning to be observed, direct pairing with renewable generation assets is also likely.

In the model, we address intermittency by modeling simple scenarios for the the adoption of batteries, avoiding modeling the dynamic stochastic problem of storage directly. We assume each unit of renewable capital must be paired with battery storage in a range of capacities. We also assume battery storage costs also follow a learning by doing process, in which their production costs fall as output expands. The baseline case assumes zero battery storage requirements. We provide more details in Section 4.5. There we also consider capacity payments to fossil fuel capital.

2.5 A Spatial Economy with Power

We embed the energy sector in a dynamic multi-region, multi-sector spatial economy. The consumer has Cobb-Douglas preferences over goods from different sectors s,

$$C_{j,t} = \prod_s C_{js,t}^{\beta_{js}}$$

where β_{js} is the consumption share of region j in sector s.

For each sector s each region j produces a differentiated good as in Armington (1969) and these goods are aggregated through a standard constant elasticity aggregator with an elasticity across varieties σ_s. Labor is fully mobile across sectors within the regions and we denote the wage rate in region j by w_j.

The production of the differentiated good for the amount the regional good j is given by

$$q_{js,t} = z_{js,t} \left(e^1_{js,t}\right)^{v^{\mathcal{E}}_{is}} \left(\kappa_{js,t}\left(e^2_{js,t}\right)^{\frac{\psi-1}{\psi}} + f^{\frac{\psi-1}{\psi}}_{js,t}\right)^{\frac{\psi}{\psi-1}v^{\mathcal{F}}_{is}} k^{v^K_{is}}_{js,t} L^{v^L_{is}}_{js,t}$$

where for each region j, sector s, and time t, $z_{js,t}$ is a regional productivity shifter, $L_{js,t}$ is the amount of labor used, $e^1_{js,t}$ is the direct amount of electricity used in production, and $e^2_{js,t}$ is secondary use of electricity that is directly substitutable with the additional use of fossil fuels $f_{j,s}$. The production capital is denoted by $k_{js,t}$. We assume that $v^{\mathcal{E}}_{is} + v^{\mathcal{F}}_{is} + v^K_{is} + v^L_{is} = 1$ for all i and s. Lastly, there is an iceberg trade cost $\tau_{ij,s}$ for shipping a unit of the good from i to j in sector s.

Given a price for electricity $p^{\mathcal{E}}_{j,t}$, wages in location j, w_j, and and a price for fossil fuels, the demand for electricity in region j sector s $\tilde{D}_{js,t}$ comes from the cost minimization problem of the firm, and satisfies

$$\tilde{D}_{js,t} = \left(p^{\mathcal{E}}_{j,t}\right)^{-1} w_j L_{js} \frac{v^{\mathcal{E}}_{is}}{v^L_{is}} \left(1 + \frac{v^{\mathcal{F}}_{is}}{v^{\mathcal{E}}_{is}}\right) \tag{10}$$

and total demand for electricity in j is $D_{j,t} = \sum_s \tilde{D}_{js,t}$. The price of the regional good from i in j is

$$p_{ijs,t} = \frac{\tau_{ijs,t}}{z_{is,t}} w^{v^L_s}_{i,t} (p^{\mathcal{E}}_{i,t})^{v^{\mathcal{E}}_{is}+v^{\mathcal{F}}_{is}} \left(r^K_{i,t}\right)^{v^K_{is}} \left(\kappa_{is,t} + \left(\frac{\kappa_{is,t}p^{\mathcal{F}}_{i,t}}{p^{\mathcal{E}}_{i,t}}\right)^{1-\psi}\right)^{-\frac{\psi}{\psi-1}v^{\mathcal{F}}_{is}} \tag{11}$$

Total sales for each sector, region, denoted by $X_{is,t}$ are given by

$$X_{is,t} = \sum_j p_{ijs,t} Y_{ijs,t} = \sum_j \frac{p^{1-\sigma}_{ijs,t}}{\left(P^{\mathcal{C}}_{js,t}\right)^{1-\sigma}} \beta_{j,s} E_j \tag{12}$$

where $P^{\mathcal{C}}_{js,t} = \left(\sum_i p^{1-\sigma_s}_{ijs,t}\right)^{1/(1-\sigma_s)}$ is the CES Dixit-Stiglitz price index.

13

Given that production of the final good is competitive, it must be true that for each time t for each region i and sector s we have

$$X_{i,t} = \sum_s X_{is,t} = \underbrace{w_{i,t}L_{i,t}}_{\text{labor income}} + p_{i,t}^{\mathcal{E}}D_{i,t} + r_{i,t}^K \sum_s k_{is,t} \tag{13}$$

Expenditure in a location is

$$E_{i,t} = \underbrace{w_{i,t}L_{i,t}}_{\text{labor income}} + p_{i,t}^{\mathcal{E}}Y_{i,t}^{\mathcal{E}} - p_t^{\mathcal{F}}F_{i,t} + \Pi_{i,t}^{\mathcal{T}} \tag{14}$$

where F_i is the use of fossil fuels in electricity production.

We show in the Appendix that if the electricity utility attempts to solve the problem in (9), where the $Q(\cdot)$ function is total regional output in dollars, $Q(p_{i,t}^{\mathcal{E}}) = \sum_s p_{is,t}q_{is,t}$, the competitive allocation that results is optimal within period.

3 Renewables Investment and Clean Growth

To analyze the growth of renewables, we now introduce investment in electricity generation capital. We also explicitly introduce time, which is discrete and indexed by t, and characterize consumer and firm intertemporal choices.

Our baseline analysis assumes that new fossil-fuel capital is uneconomic. For the developed world, this not an unreasonable assumption: . Such an assumption is also consistent with the commitments from 40 economies in the 2022 United Nations climate change conference and 2022 G7 meeting of ending public support to fossil fuel projects by the end of 2022 except in "limited and clearly defined circumstances that are consistent with a 1.5°C warming limit and the goals of the Paris Agreement".

The law of motion of renewable capital is

$$K_{j,t+1}^{\mathcal{R}} = (1-\delta)K_{j,t}^{\mathcal{R}} + Q_{j,t+1}^{\mathcal{R}}. \tag{15}$$

We suppose that renewable capital can be produced by transforming $I_{j,t}^{\mathcal{R}}$ units of the

final good into capital according to

$$Q_{j,t}^{\mathcal{R}} = \left(\sum_{j'} \sum_{i=1}^{\infty} (\mu)^i Q_{j',t-i}^{\mathcal{R}} \right)^{\gamma} I_{j,t}^{\mathcal{R}},$$

where $I_{j,t}^{\mathcal{R}}$ is denominated in units of the final good in j. There is a spillover into local capital production from global production in all previous periods, by which it becomes cheaper to produce a unit of renewable capital if more has been installed worldwide. $\mu < 1$ is a parameter that discounts learning from the past. The parameter γ is termed the *learning rate.* This is a "learning-by-doing" formulation with frictionless spillovers across regional borders. While no doubt an approximation, it is helpful to consider the knowledge spillovers as being mostly global and largely exogenous to local decisions. We assume that consumer invest in renewable capital and describe this problem next.

Consumer Intertemporal Choice. Units of the final good can be converted to production capital in a putty-clay formulation. Preferences of the household are

$$U_j = \sum_{t=0}^{\infty} \beta^t \log(C_{j,t})$$

subject to expenses on goods, renewable energy capital, and fossil fuel assets. The budget constraint is given by

$$P_{j,t}^{\mathcal{C}} C_{j,t} + P_{j,t}^{\mathcal{C}} I_{j,t+1}^{\mathcal{R}} + P_t^{\mathcal{A}} a_{j,t+1} = E_{j,t} + a_{j,t} \tag{16}$$

where $a_{j,t}$ is the saving in location r in a global, risk-free bond, $P_t^{\mathcal{A}}$ is the price of the savings bond to yield 1 unit next period (normalized in terms of the price of the world numeraire) and we assume that bond markets clear in each period

$$\sum_j a_{j,t} = 0. \tag{17}$$

The first order conditions of the household with respect to consumption and savings imply an

Euler equation for consumption,

$$\frac{C_{j,t+1}}{C_{j,t}} = \beta \frac{1}{P_t^{\mathcal{A}}} \frac{P_{j,t}^{\mathcal{C}}}{P_{j,t+1}^{\mathcal{C}}} \tag{18}$$

15

where we can define the real interest rate as

$$1 + r_{j,t} \equiv \frac{1}{P_t^{\mathcal{A}}} \frac{P_{j,t}^{\mathcal{C}}}{P_{j,t+1}^{\mathcal{C}}} \tag{19}$$

which is potentially different across regions due to changing final goods prices.

Renewable Capital Investment. Owing to the fact that the marginal cost of renewables is zero and the investment is modular, the value of a unit of renewable capital, once installed is given by

$$V_{j,t}^{\mathcal{R}} = p_{j,t}^{\mathcal{E}} \theta_j + \frac{1-\delta}{(1+r_{j,t})} V_{j,t+1}^{\mathcal{R}}.$$

We assume that there is free entry of investors in renewables, in each region (as in Walsh (2021)). Now we can use the fact that in any two periods with positive renewable capital investment, the price of a unit of renewable capital must equal the value, $V_{j,t}^{\mathcal{R}} = p_{j,t}^{\mathcal{R}}$, so that

$$p_{j,t}^{\mathcal{R}} = p_{j,t}^{\mathcal{E}} \theta_j + \frac{1-\delta}{1+r_{j,t}} p_{j,t+1}^{\mathcal{R}} \tag{20}$$

where

$$p_{j,t}^{\mathcal{R}} = \left(\sum_{j'} \sum_{i=1}^{\infty} (\mu)^i Q_{j',t-i}^{\mathcal{R}} \right)^{-\gamma} P_{j,t}^{\mathcal{C}}. \tag{21}$$

where $\mu < 1$ and captures knowledge decay. Given capital prices, the price of electricity, $p_{j,t}^{\mathcal{E}}$, is pinned down by this law of motion. This in turn determines electricity production $Y_j^{\mathcal{E}}$, and consumption, D_j.

We are now ready to define a dynamic spatial equilibrium with electricity production.

Definition 1. *An equilibrium is a vector of wages $\{w_{j,t}\}$, a bond price $\{P_t^{\mathcal{A}}\}$, prices of electricity $\{p_{j,t}^{\mathcal{E}}\}$, prices of the renewable capital $\{p_{j,t}^{\mathcal{R}}\}$, allocations of the final good $\{C_{j,t}\}$, and renewable capital stock $\{K_{j,t}^{\mathcal{R}}\}_t$ such that for each location j and time period t:*

i) the wages $\{w_{j,t}\}$ satisfy the goods market clearing condition (equation (12)) ii) the bond market clears (equation (17)) iii) The price of electricity $\{p_{j,t}^{\mathcal{E}}\}$ satisfies equation solves (9) where

production of electricity $\left\{Y_{j,t}^{\mathcal{E}}\right\}$, demand for electricity $\{D_{j,t}\}$ are given by (3) and (10) and the law of motion (15). iv) the price of the renewable capital $\{p_{j,t}^{\mathcal{R}}\}$ evolves according to (21), v) intertemporal consumption choices $\{C_{j,t}\}$ satisfy (18) vi) investment in renewables and the associated capital stock $\{K_{j,t}^{\mathcal{R}}\}_t$ satisfy the free entry condition (equation (20)) if $I_{j,t+1}^{\mathcal{R}} > 0$.

A steady state equilibrium is an equilibrium in which all variables are constant. In the appendix we characterize the computational algorithm for the solution of this system.

4 Quantitative Analysis

For our quantitative analysis we consider a set of sub-national geographies that roughly correspond to local labor market areas. To do so, we harmonize datasets from different sources so that they correspond to those geographies. Our regions correspond roughly to commuting areas in the US, and NUTS-3 regions in most of European countries. For other countries we attempt the most granular level of aggregation possible, depending on the available data.

The harmonization procedure constitutes of bringing together datasets from three disparate sets of sources. Data from the electricity grid and power assets, data for output and employment, and regional trade data.

4.1 Global Power Grid and Electricity Generation

We first construct a unified dataset on the global electricity grid. We source data on the length and voltage of high-voltage transmission lines from OpenStreetMap. A full description of our methods for processing the raw data is contained in Appendix A2. Data on global power generation assets comes from the World Resources Institute Database. It contains information on the size of the power plant, the location, the date constructed and the type of fuel and detailed location information. A summary of this data is provided in Appendix A2.

We then construct a simplified representation of the electricity dataset. First, we aggregate transmission capacity between each region. We sum the total capacity of all lines

Figure 4: North American Electricity Grid and Power Generation Assets
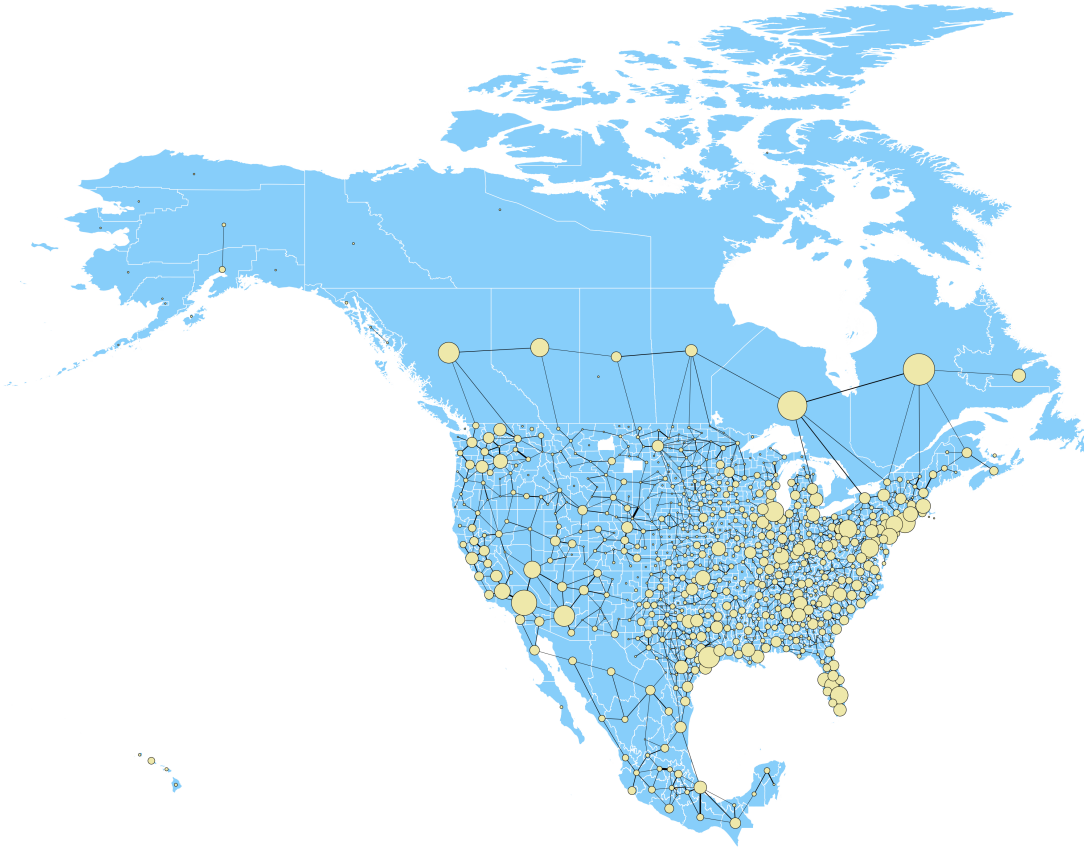
Notes: This figure shows a representation of the electrical grid between regions of North America using data from Openstreetmap (transmission lines) and the World Resources Institute Database (power capital). Circle size is proportional to region generating capacity in MW. Line thickness is proportional to the number of transmission lines between regions

which begin in one region and end in another, and compute the distance of transmission as stretching from region centroid to region centroid. Lines which begin and end in the same region are dropped. We then add the total fossil-fuel capacity and renewable capacity (by type) separately, and consider all generation to be done at the region centroid. [4] We code hydro-electricity plants, coal, gas and nuclear as fossil-fuels $\mathcal{F}$,[5] and consider renewables to be solar and wind. The result for North America is presented in Figure 4, and other major regions are presented in the Appendix.

---

[4]Note that as the regional partition becomes finer, this method of representation will approach the true dataset.

[5]We do this given their similar economics of large fixed costs and variable fuel costs, and not for their role in emitting CO2.

As specified above, we assume renewable generation capacity has zero marginal cost, and the productivity of the asset is determined by the renewable potential in the area and the data. We average both daily solar insolation and daily wind speeds within a location, using data from the Global Solar Atlas and the Global Wind Atlas as displayed in Figures 2a and 2b by our national sub-divisions. Power generation using fossil assets is extracted from data from the World Resources institute, depicted in the bottom panel of 4 for the US.

Finally, we model the fossil fuel sector as operating outside of the rest of the economy and construct the global fossil fuel supply curve by computing the global price of fossil fuels as a function of quantity demand $p^{\mathcal{F}}(F)$. We use data from Asker et al. (2019) for the unit costs for each quantity supplied for major oil suppliers. For each oil supplier we compute the improvements in the productivity of oil extraction from 1990-2010 for different quantities. We assume these improvements continue in the future and use the implied relative wages predicted from our model to compute the unit cost for each country and the resulting global supply curve in the different counterfactual scenarios for different years.

4.2 Production, Employment, and Trade Data

Our main data source for regional value added sectoral and employment data is the OECD iLibrary, which includes regional economic and demographic data per year at two different levels of territorial aggregation called territorial levels (TL): TL3 and TL2.[6] The large TL2 regions correspond to political boundaries similar to states. In contrast, smaller TL3 regions, which are contained within in a TL2 region, are similar to counties or commuting zones as discussed above for the US and EU. Whenever possible we aim for TL3 region and opt for additional data sources if these are not directly available through OECD. For our calibration we use data for 2015 because in this the latest year where most of the countries had the least amount of missing data by industry. After our selection process and the additions from other datasets we end up –as of now– with a total of 40 countries and 1914 regions. We depict the regional and national borders in Figure 5. We use these variables in current US dollars adjusted by Purchase Power Parity. Moreover, Gross Value Added and employment are disaggregated by industry

---

[6]We discuss the details of all the construction of the production, employment, and trade data, in our online data appendix.

Figure 5: World Regions
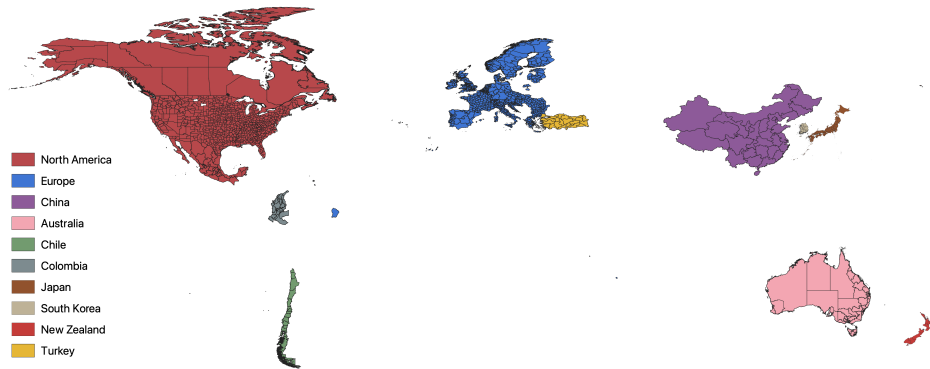
Notes: This figure shows the selected regions for the world, with colors indicating the zones we treat as integrated grids.

following the High-level SNA/ISIC aggregation (A*10), that groups economic activities in ten different sectors.[7]

To calibrate the trade costs of the model, we measure trade frictions using regional trade data aggregated at the same ten sectors as the gross value added and employment data. The data are based on the EUREGIO Regional Input-Output database (see Thissen et al. (2018)). The survey determines trade flows of different types of goods between regions in Europe and some non European countries, by surveying all possible modes of transport.[8] We aggregate the data to our geographic regions to create a precise mapping to our employment data. Similarly so we aggregate as close as possible to the 10 different sectors of the OECD dataset, which due to the differences in the datasets, results in 8 sectors.[9]

To estimate trade costs, we postulate that they are given by

---

[7]This data can be found in https://www.oecd-ilibrary.org/urban-rural-and-regional-development/data/oecd-regional-statistics_region-data-en. The ten ISIC revision 4 sectors we aggregate the data to are i. Agriculture, forestry and fishing, Manufacturing, ii. mining and quarrying and other industrial activities, iii. Construction iv. Wholesale and retail trade, transportation and storage, Accommodation and food service activities, v. Information and communication vi. Financial and insurance activities vii. Real state activities viii. Professional, scientific, technical, administrative and support service activities ix. Public administration and defence, education, human health and social work activities x. Other service activities

[8]These modes include land traffic (by trucks), rail transport, air transport, freight transport, and non-motorized passenger transport.

[9]We estimate the same coefficient for Real state and Professional, scientific, technical, administrative and support service activities and Public administration as well as for defence, education, human health and social work activities and Other service activities.

$$\tau_{ijs} = e^{\omega_s} \left(\mathcal{B}_{inter}\right)^{\mathbb{1}_{C_i \neq C_j}} \left(\mathcal{B}_{intra}\right)^{\mathbb{1}_{i \neq j, C_i = C_j}} \left(d_{ij}\right)^{\beta_s}. \tag{22}$$

distance d_{ij}, an intra-country border cost, $\left(\mathcal{B}_{intra}\right)^{\mathbb{1}_{i \neq j, C_i = C_j}}$, an inter-country border cost, $\left(\mathcal{B}_{inter}\right)^{\mathbb{1}_{C_i \neq C_j}}$, and a sector-specfic cost e^{ω_s}. Taking logs we can recover the trade cost components by estimating the following gravity regression

$$\ln\left(X_{ijs}\right) = (1 - \sigma) \ln\left(\mathcal{B}_{intra}\right) \mathbb{1}_{i \neq j, C_i = C_j} \tag{23}$$

$$+ (1 - \sigma) \ln\left(\mathcal{B}_{inter}\right) \mathbb{1}_{C_i \neq C_j} \tag{24}$$

$$+ \sum_{s=1}^{S} (1 - \sigma)\beta_s \ln\left(d_{ij}\right) \mathbb{1}_s + \omega_i + \omega_j + \omega_s + \epsilon_{isj} \tag{25}$$

where X_{ijs} is the value of the trade flow from region i, sector s, to region j, $\mathbb{1}_s$ is an indicator that takes the value of 1 when the sector is s, $\mathbb{1}_{i \neq j, C_i = C_j}$ is an indicator variable that takes the value of 1 if regions i and j belong to the same country (and are not the same region), $\mathbb{1}_{C_i \neq C_j}$ is an indicator variable that takes the value of 1 if regions i and j belong to different countries, d_{ij} is the distance regions i and j, and ω_i, ω_j, and ω_s are fixed effects for region of origin, destination region, and origin sector, respectively.

The estimates are reported in Table 1. We report three salient findings. First, the coefficient on log distance differs across sectors, with intuitive deviations from the coefficient of -1 that commonly appears in aggregated gravity regressions (see e.g. Head and Mayer (2014)). The coefficient on construction is -2.11, while the coefficient on information and communication only a quarter of that, -0.56. The coefficient on various tradeable services (Financial and insurance activities as well as Real state activities/ Professional, scientific, technical, administrative and support service activities) is somewhat low, below -0.78. Rerunning the regression aggregated across sectors indeed yields a coefficient very close to -1 (-1.01), and running the regression aggregated across countries for the ten sectors also results to coefficient much closer to one. Second, the effects of the borders are large, and amount to a doubling of the distance multiple times. Third, not surprisingly, the inter-country borders are affecting trade much more than intra-country borders.

Table 1: Gravity regression estimates: 8 SNA/ISIC sectors

Variable	(1)	(2)
$\ln\left(Distance_{ij}\right)$		
Agriculture, forestry and fishing, manufacturing	−0.915***	−0.890***
	(0.009)	(0.013)
Mining, quarrying and other industrial activities	−0.433***	−0.865***
	(0.009)	(0.011)
Construction	−1.459***	−2.090***
	(0.009)	(0.019)
Wholesale and retail trade, transportation	−1.036***	−1.284***
and storage, Accommodation and food service activities	(0.009)	(0.014)
Information and communication	−0.773***	−0.573***
	(0.009)	(0.011)
Financial and insurance activities	−1.370***	−0.767***
	(0.009)	(0.016)
Real estate/Professional, scientific, technical,	−0.929***	−0.733***
administrative and support service activities	(0.009)	(0.014)
Public administration and defence, education,	−1.118***	−0.837***
human health and social work activities/other service activities	(0.009)	(0.014)
Intra-Country Border	−4.189***	−4.193***
	(0.056)	(0.062)
Inter-Country Border	−7.435***	−7.435***
	(0.058)	(0.064)
Industry FE		✓
Region of origin FE	✓	✓
Destination region FE	✓	✓
Observations	542,771	542,771
R^2	0.56	0.57

Coefficients are estimates for the regression of (log) trade flow between regions on the distance between regions interacted with an origin sector dummy, a dummy for different regions, and a dummy for different countries. Regression includes fixed effects for region of origin, destination region, and industry in origin region. Each observation is a tuple origin region-origin industry-destination region. Origin industry codes are 8 different sectors obtained by mapping GSV sectors to their SNA/ISIC counterparts. Robust standard errors in parenthesis. All numbers rounded to the nearest thousandth. * $p < 0.1$, ** $p < 0.05$, *** $p < 0.01$.

4.3 Calibration

We use our estimated sectoral trade costs to calibrate the trade costs in the model, $\tau_{ij,s}$, using centroid to centroid distances of our regions. We target the employment shares by region-sector and the regional output to calibrate the productivities of the model for each sector, z_{is}, using the full equilibrium structure of the model (Allen and Arkolakis (2014); Redding and Rossi-Hansberg (2017)).

To calibrate factor shares in the final product firms' production function we use data from the Global Trade Analysis Project (henceforth, GTAP) global input-output (IO) table, which features 65 sectors in 141 countries. To accommodate our sector definition we proceed by mapping each of the GTAP sectors to our 10 SNA/ISIC sectors. Using this data, we compute factor shares for fossil fuels, $v_i^{\mathcal{F}}$, for electricity, $v_i^{\mathcal{E}}$, for capital, $v_i^{\mathcal{K}}$, and labor $v_i^{\mathcal{L}}$, by dividing the expenditures on each factor for a given sector-country by the total sectoral expenditures in that country. To obtain total expenditures in each of these factors, we proceed as follows. For capital and labor, we use factor endowments directly. For fossil fuels and electricity, we label each of the original GTAP sectors as fossil fuels sectors, electricity sectors, or neither. Then, we compute spending from the intermediate input trade data as total expenditure by each sector s in country c on fossil fuel sectors and electricity sectors, respectively.

We specify the production function for $Y_j^{\mathcal{E}}$ as

$$Y_j^{\mathcal{F}} = (K_j^{\mathcal{F}})^{\alpha} F_j^{1-\alpha}, \quad Y_j^{\mathcal{F}} \leq \bar{Y}_j^{\mathcal{F},max}.$$

We choose $\alpha = 0.04$ to match a marginal cost curve of fossil fuel electricity that rises slowly with increased power output, roughly matching the slope of marginal cost curves in PJM and other major power markets in the US (see Sahraei-Ardakani et al. (2015)).[10] Maximum output in a region $\bar{Y}_j^{\mathcal{F},max}$ is given by summing the rated capacity of all fossil assets with a region in the data. We use the information on the line length and voltage to construct a value of the resistance for each line in the model by dividing the length (which is measured in centroid to centroid distance if two regions are connected by transmission lines in the data) by the rated voltage in the data.

---

[10]One limitation of this specification is that it is not able to capture sharp convexities in marginal cost that are seen when regions are operating at peak output due to the use of gas and oil peaker plants.

To calibrate the learning rate of renewable capital, we use data from the International Renewable Energy Agency (IRENA) on the average total installed cost of wind and solar power. We estimate a regression of the form

$$\log(\text{Total Cost}_t) = \alpha + \gamma \log(\text{Total Installation}_t) + \epsilon_t$$

separately by technology. The results are plotted in Figure (A3), and yield a value of 0.6 for solar and $\gamma = 0.27$ for onshore wind. We choose $\gamma = 0.4$ to balance these two estimates, and explore sensitivity of the results to different learning rates.

To calibrate renewable potential θ_r, we average annual solar insolation and wind potential within each region j, and normalize these to a reference cell. We then take θ_r to be the max of these two values, reflecting that some regions are particularly suited to solar, and some to wind. Lastly, we apply a capacity factor of 30% for renewable capacity, which is in line with recent estimates from the literature. This capacity factor directly multiplies θ_r in each region, and lowers the expected amount of electricity in an annual period generated from a unit of capital by the capacity factor.

There are four remaining parameters that we externally calibrate. We set the depreciation of renewable capital to 3% based on the low degradation rates of new renewable photovoltaic and wind turbines that are expected to last thirty years or more (Jordan and Kurtz (2013); Wiser and Bolinger (2019)). We set the long run interest rate to be 5%, and the rate of forgetting to be $\mu = 0.01$.

Lastly, a parameter which has no direct observable counterpart is ψ, the ease of substituting between direct fossil fuel use and electricity at end use, in both industry and consumption. In particular, it may differ at short and long run horizons, as it indexes the possibility of "electrification". In our baseline calibration we assume $\psi = 1.1$, and explore sensitivity of the results to various values. We use a baseline elasticity of substitution, σ, of 4, which implies a trade elasticity of 3.

4.4   Model Fit

The model does a reasonable job at reproducing spatial patterns of power prices seen in the data. We collect Locational Marginal Prices for the US from 9 Regional Transmission Organizations, and then average the hourly price at each node in the data for 2020. The

24

result is shown in Figure A5, along with the predictions of the model for the equilibrium prices in each region of the US. The states without data do not employ Locational Marginal Pricing and thus cannot be compared to our model predictions.

The higher prices in California and New England are clearly visible. The lower band of prices across the Midwest is also apparent, as are somewhat higher prices in the Rustbelt ex. upstate New York. Overall, the model can reproduce fairly well the variation in spatial prices in at least one region of the world for which we have data.

4.5 Extensions for Quantitative Analysis

We introduce two extensions to the baseline model that can partially address the intermittancy of renewables indirectly, as we have sidestepped modelling their stochastic nature.

Batteries. We assume every unit of renewable capital must be paired with a battery of size B, where size is measured in Mwh. These sizes we consider are 0, 0.5, 2 and 4 Mwh per each unit of renewable capital (recall that size is measured in MW). Batteries are produced under constant returns, and available at price $p_{j,t}^{B}$, where $p_{j,t}^{B}$ follows a learning process similar to that of capital, given by

$$p_{j,t}^{\mathcal{B}} = \left(\sum_{j'} \sum_{i=1}^{\infty} (\mu)^i Q_{j',t-i}^{\mathcal{B}} \right)^{-\gamma_B} P_{j,t}^{\mathcal{C}}.$$

where $Q_{j',t-i}^{\mathcal{B}}$ is the quantity of batteries produced. We take the learning rate for batteries γ_B to be $\gamma_B = 0.1$, roughly in line with estimates from the literature, and reflecting somewhat slower expected price declines with output due to projected supply constraints for battery materials.

Capacity Payments to Fossil Fuels. We also model direct capacity payments to fossil fuels. We assume that payments are made such that the depreciation costs of fossil fuel capital are met at 1/3 of current capacity (note this does not mean that 1/3 of long run electricity is supplied by fossil fuels). These payments are financed by lump sum taxes on workers in the regions covered by their own utility.

Figure 6: Renewable Transition Path
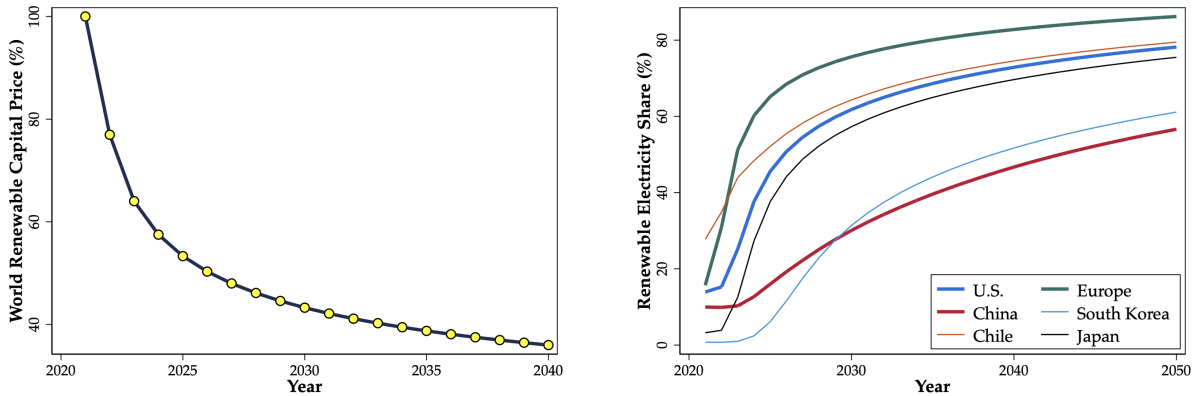
Notes: This left panel shows the model's projection for the world capital price in the baseline scenario, normalized to 100 in 2021. The right panel shows the share of electricity coming from renewables in each country or region in the baseline scenario.

5   Counterfactual Exercises

In this section, we assess the impact of renewable energy on income growth and trade patterns. We solve for a perfect foresight equilibirum, beginning with the calibrated model in 2020 and shooting forward until the model reaches a new steady state.[11]

5.1   Clean Growth Across the Globe

Figure 6 presents an aggregate summary of the energy transition. The model predicts that the aggregate price of renewable capital falls by almost 60% by 2030. While substantial, this is somewhat lower than the previous pace of price declines seen for solar. As seen in Figure A3, in the previous decade (from 2010 to 2010), the total installed price of solar capital decreased by 81%. The reason is twofold. Once capital becomes widely adopted in many regions, passing the initial threshold of no investment, proportional increases in the total stock installed worldwide begin to slow (though the learning rate γ remains unchanged). Second, we have taken a somewhat lower learning rate for renewable capital than is observed in the data for solar costs.

In Figure 7 we plot the long-run changes in real wages across countries induced by the energy transition. The biggest winners are generally countries in Europe. Initially,

---

[11]The existence of a long-run steady state is ensured by the forgetting parameter μ. Without it, perpetual price falls are possible are under certain parameter combinations.

Figure 7: Long-Run Real Wage Changes
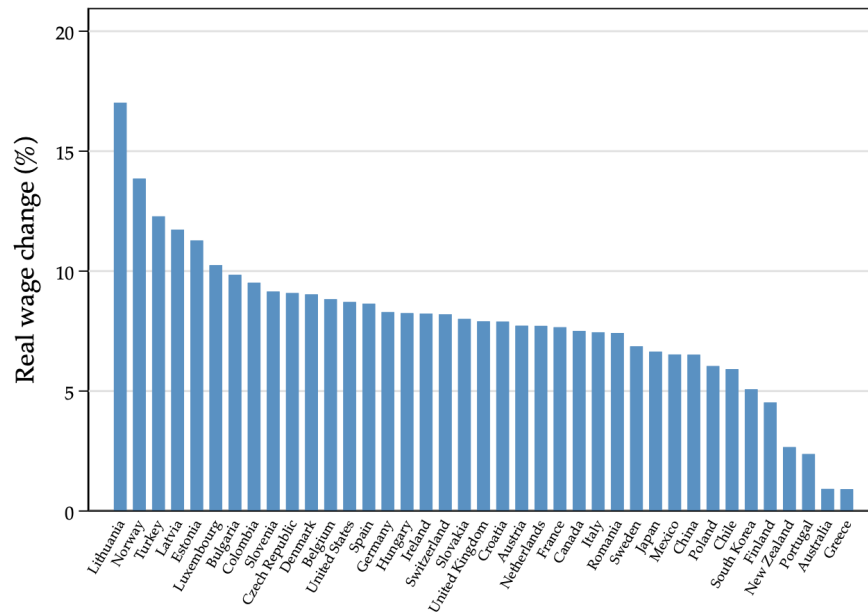
Notes: This Figure shows the model changes in real wages in the baseline scenario. We average changes in real wages at the region level weighted by local population.

this might seem counterintuitive. Countries which have poorly connected electricity infrastructure (Greece) or initial low power prices (Australia) do less well. These long-run wage changes are of a substantial magnitude. Long-run estimates of the cost of climate change are of a similar magnitude

The results are sensitive to the specification of the learning rate, and speculation whether the aggregate rate is stable and will remain at its current value for the forseeable future is reasonable. In the Appendix we explore several specifications for alternative values of the learning rate.

5.2 The Inflation Reduction Act and Renewable Subsidies

We now study the effects of a subsidy in the form of a production credit to renewable energy. In August 2022, the Biden Adminstration signed into law the Inflation Reduction Act, which contained significant spending measures designed to encourage the uptake of renewable energy. Chief among these was an production tax credit of \$26 per mWh for renewable energy from any source, extended out to 2034 (source).

Figure 8: The Impact of the Inflation Reduction Act
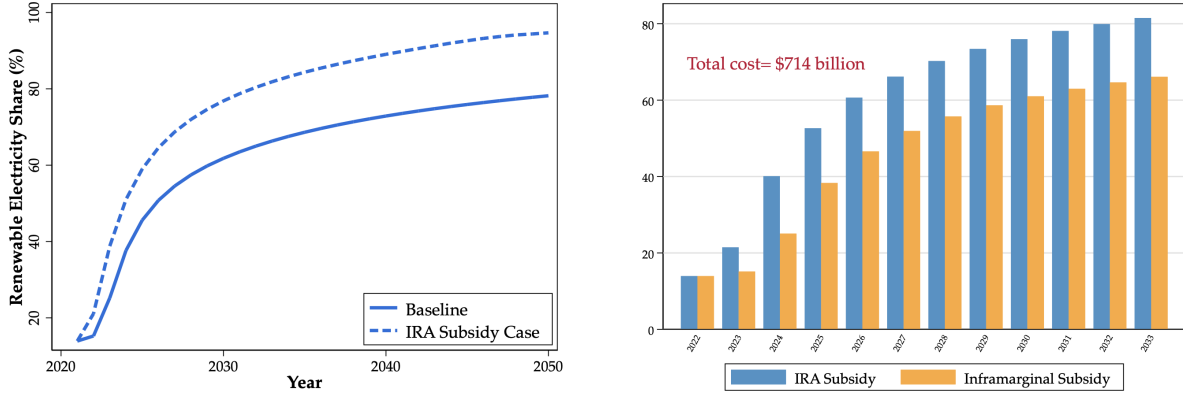
Notes: This left panel shows the model's projection for renewable power share under the IRA production tax credit, and without. The right panel shows the total cost of the bill (in blue), and subsidies going to capital that would be installed in the absence of the subsidy.

We model this by assuming that electricity produced for renewable sources receives a subsidy s_t.

$$p_{j,t}^{\mathcal{R}} = (p_{j,t}^{\mathcal{E}} + s_t)\theta_j + \frac{1-\delta}{1+r_{j,t}}p_{j,t+1}^{\mathcal{R}}$$

The subsidy is funded by labor income taxes on all regions in the US, with a time varying (but spatially invariant) rate τ_t, which solves

$$\sum_{j \in US} w_{j,t} L_j (1 - \tau_t) = s_t \sum_{j \in US} Y_j^{\mathcal{E}}$$

There are no taxes in the model, and thus directly comparing this to the electricity revenue received by a unit of renewable capital is not immediate. We proceed as follows. We first note that $26 is around 60% of the average wholesale price prevailing in markets with locational market prices in 2020, and set the value of s_t in the model to be 60% of the average equilibrium 2020 $p_t^{\mathcal{E}}$ in the US. We assume that the subsidy is removed after 2034, and goes to zero in 2035. We solve for the counterfactual global equilibrium, holding all other regional fundamentals constant.

The results are presented in Figure 8. The production tax credit induces signifcant uptake of renewable energy in the US over and above the baseline case. Instead of reaching 60% of production by 2030, the renewable share is 78%. The credit goes some way to accelerating world-wide adoption, modestly increasing . This is because the US

is a substantial buyer of renewable capital, and accelerating adoption plans increases world production of capital, putting downward pressure on the price via learning by doing.

It is worth noting that in the model, this production credit can have only transitional effects. This is due to the forgetting rate μ, which discounts production in the far past in affecting the price of capital today. As such, the IRA cannot effect the long run steady of the model, as infinitely far into the future its effects have been lost. It only has transitional effects, speeding up adoption in the movement towards the long run steady state.

The costs of the IRA are substantial. The IRA bill budgets for \$160 billion in spending on this production tax credit. We find instead that around \$714 billion is spent before the subsidy expires in 2034. Over 87% of this total goes to subsidizing inframarginal investment, or investment that would have happened absent the subsidy.

6   Conclusions

We have developed a spatial theory of clean growth to assess the global rise of renewable energy. We find that continued growth in renewable installation is likely to lead to substantial falls in the price of power, with widespread benefits to production and real wages. All countries benefit from this technological shift, though the long run effect depends on initial power prices and the strength of the transmission network.s Production based subsidies of the kind seen in the US can substantially accelerate the renewable energy transition, though may come at substantial cost.

References

Allen, Treb and Costas Arkolakis, "Trade and the Topography of the Spatial Economy," *The Quarterly Journal of Economics*, 2014, *129* (3), 1085–1140. [23]

Alvarez, Jose Luis Cruz and Esteban Rossi-Hansberg, "The economic geography of global warming," Technical Report, National Bureau of Economic Research 2021. [4]

Anderson, James E., "A Theoretical Foundation for the Gravity Equation," *American Economic Review*, 1979, *69* (1), 106–116. [1]

Armington, Paul S., "A Theory of Demand for Products Distinguished by Place of Production," *International Monetary Fund Staff Papers*, 1969, *16*, 159–178. [1, 13]

Asker, John, Allan Collard-Wexler, and Jan De Loecker, "(Mis) allocation, market power, and global oil extraction," *American Economic Review*, 2019, *109* (4), 1568–1615. [4, 19]

Benthem, Arthur Van, Kenneth Gillingham, and James Sweeney, "Learning-by-doing and the Optimal Solar Policy in California," *The Energy Journal*, 2008, *29* (3). [1]

Bohn, Roger E, Michael C Caramanis, and Fred C Schweppe, "Optimal pricing in electrical networks over space and time," *The Rand Journal of Economics*, 1984, pp. 360–376. [A7]

Conte, Bruno, Klaus Desmet, Dávid Krisztián Nagy, and Esteban Rossi-Hansberg, "Local Sectoral Specialization in a Warming World," *Journal of Economic Geography*, 2021, *21* (4), 493–530. [4]

Costinot, Arnaud and Andrés Rodríguez-Clare, "Trade theory with numbers: Quantifying the consequences of globalization," in "Handbook of international economics," Vol. 4, Elsevier, 2014, pp. 197–261. [3]

Fröling, Maria, "Energy use, population and growth, 1800–1970," *Journal of Population Economics*, 2011, *24* (3), 1133–1163. [3]

Golosov, Mikhail, John Hassler, Per Krusell, and Aleh Tsyvinski, "Optimal taxes on fossil fuel in general equilibrium," *Econometrica*, 2014, *82* (1), 41–88. [4]

Head, Keith and Thierry Mayer, "Gravity equations: Workhorse, toolkit, and cookbook," in "Handbook of international economics," Vol. 4, Elsevier, 2014, pp. 131–195. [21]

Hodgson, Charles, *Information externalities, free riding, and optimal exploration in the uk oil industry*, SIEPR, Stanford Institute for Economic Policy Research, 2019. [4]

Jordan, Dirk C and Sarah R Kurtz, "Photovoltaic degradation rates—an analytical review," *Progress in photovoltaics: Research and Applications*, 2013, *21* (1), 12–29. [24]

Kortum, Samuel S and David A Weisbach, "Optimal unilateral carbon policy," 2021. [4]

Krusell, Per and Anthony A Smith Jr, "Climate change around the world," Technical Report, National Bureau of Economic Research 2022. [4]

McDonald, Alan and Leo Schrattenholzer, "Learning Rates for Energy Technologies," *Energy policy*, 2001, *29* (4), 255–261. [1]

Mulder, FM, "Implications of Diurnal and Seasonal Variations in Renewable Energy Generation for Large Scale Energy Storage," *Journal of Renewable and Sustainable Energy*, 2014, *6* (3), 033105. [12]

Nykvist, Björn and Måns Nilsson, "Rapidly Falling Costs of Battery Packs for Electric Vehicles," *Nature Climate Change*, 2015, *5* (4), 329–332. [12]

Redding, Stephen J and Esteban Rossi-Hansberg, "Quantitative spatial economics," *Annual Review of Economics*, 2017, *9*, 21–58. [3, 23]

Rubin, Edward S, Inês ML Azevedo, Paulina Jaramillo, and Sonia Yeh, "A Review of Learning Rates for Electricity Supply Technologies," *Energy Policy*, 2015, *86*, 198–218. [1]

Sahraei-Ardakani, Mostafa, Seth Blumsack, and Andrew Kleit, "Estimating Zonal Electricity Supply Curves in Transmission-constrained Electricity Markets," *Energy*, 2015, *80*, 10–19. [23]

Stern, David I, "Energy and economic growth," in "Routledge Handbook of Energy Economics," Routledge, 2019, pp. 28–46. [3]

Tahvonen, Olli and Seppo Salo, "Economic growth and transitions between renewable and nonrenewable energy resources," *European Economic Review*, 2001, *45* (8), 1379–1398. [3]

Tangerås, Thomas and Frank Wolak, "Locational Marginal Network Tariffs for Intermittent Renewable Generation," *Available at SSRN 3495488*, 2019. [4]

Thissen, Mark, Maureen Lankhuizen, Frank van Oort, Bart Los, and Dario Diodato, "EUREGIO: The construction of a global IO DATABASE with regional detail for Europe for 2000–2010," 2018. [20]

Walsh, Conor, "Local Growth Policy and Dynamic Misallocation," 2021. [3, 16]

Wiser, Ryan H and Mark Bolinger, "Benchmarking anticipated wind project lifetimes: Results from a survey of US wind industry professionals," Technical Report, Lawrence Berkeley National Lab.(LBNL), Berkeley, CA (United States) 2019. [24]

Wolak, Frank A, "Financing the Energy Transition in a Low-Cost Intermittent Renewables Environment," 2021. [4]

A1 Additional Figures

In this section we provide additional figures to the paper. Figure A1 plots the raw power station data and transmission line data over the globe. Figure A2 plots the representation of this data for Europe and China which we use in the model. Figure A3 plots the aggregate learning rates for solar and wind capital in the data. Figure A4 plots some stylized network representations. Figure A5 plots Locational Marginal Prices for the US in 2020, as well as the model generated prices in each one of the US regions in 2020.

Figure A1: Global Electricity Infrastructure

(a) Power Capital
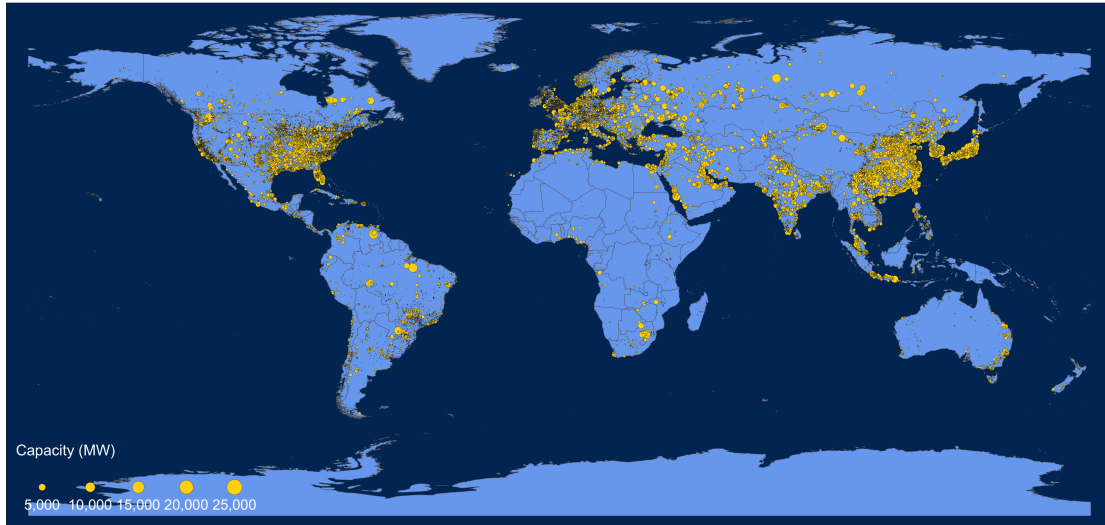
(b) Transmission Lines
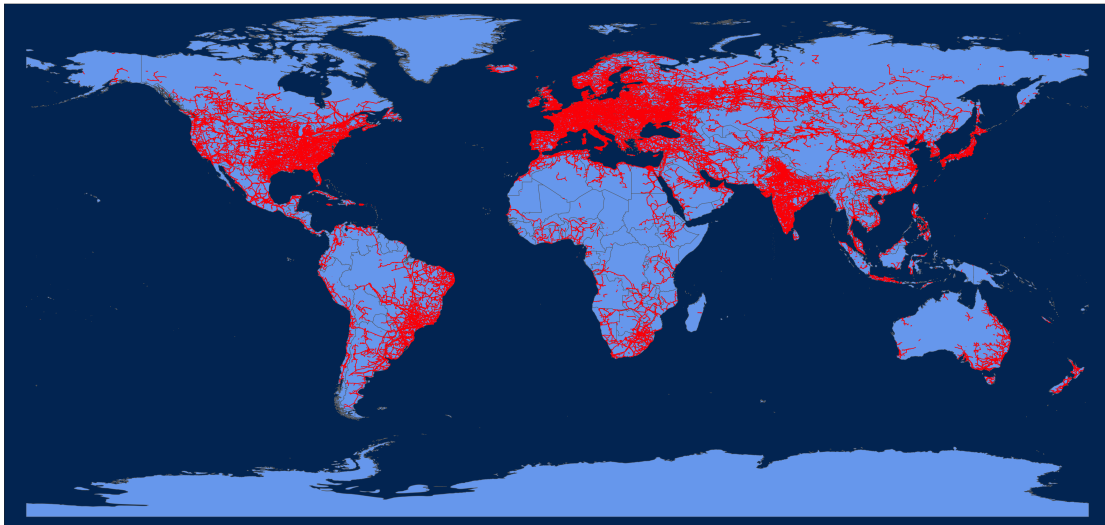
Notes: Panel (A) shows installed power capital in MW using data from the World Resources Institute. Panel (B) shows high-voltage transmission lines scraped from OpenStreetMap.

Figure A2: Network Representations for Other Major Regions

(a) China
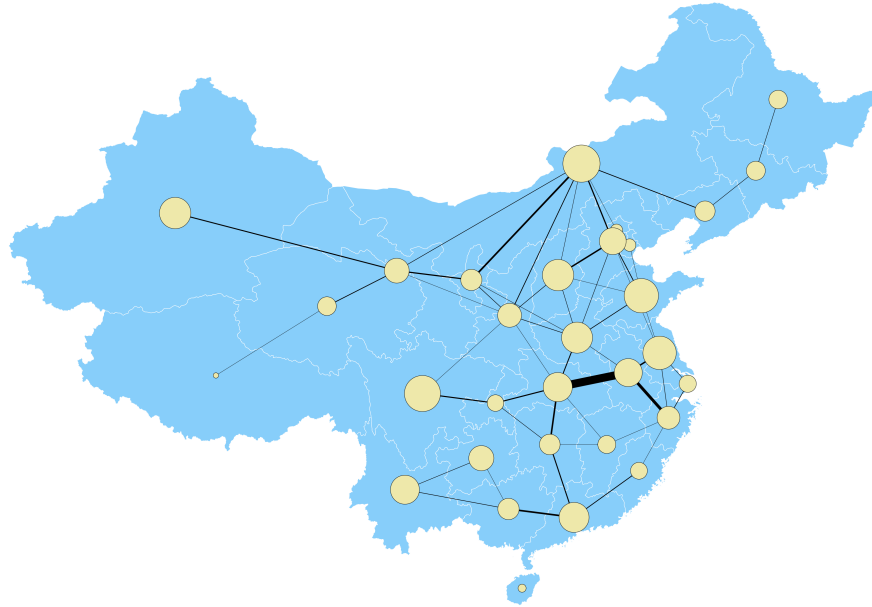
(b) Europe
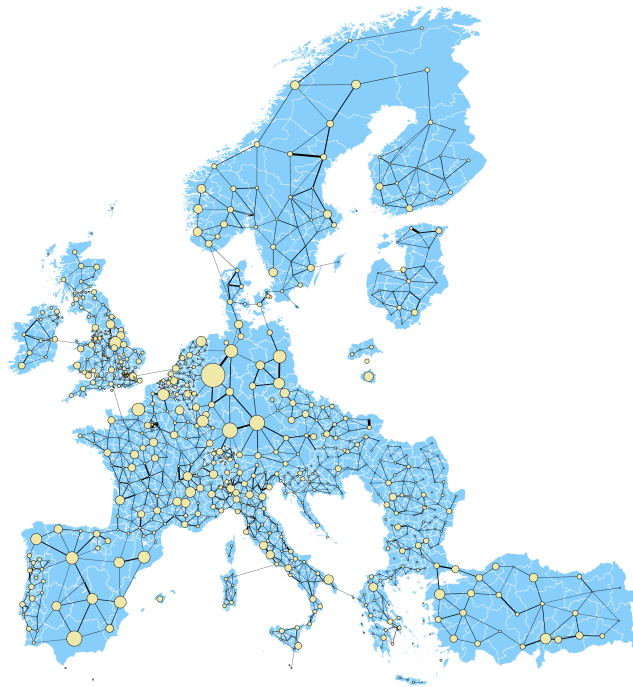
Notes: This figure shows a representation of the electrical grid between regions of China (Panel (a)) and Europe (Panel (b)) using data from Openstreetmap (transmission lines) and the World Resources Institute Database (power capital). Circle size is proportional to region generating capacity in MW. Line thickness is proportional to the number of transmission lines between regions

Figure A3: Aggregate Learning Rates
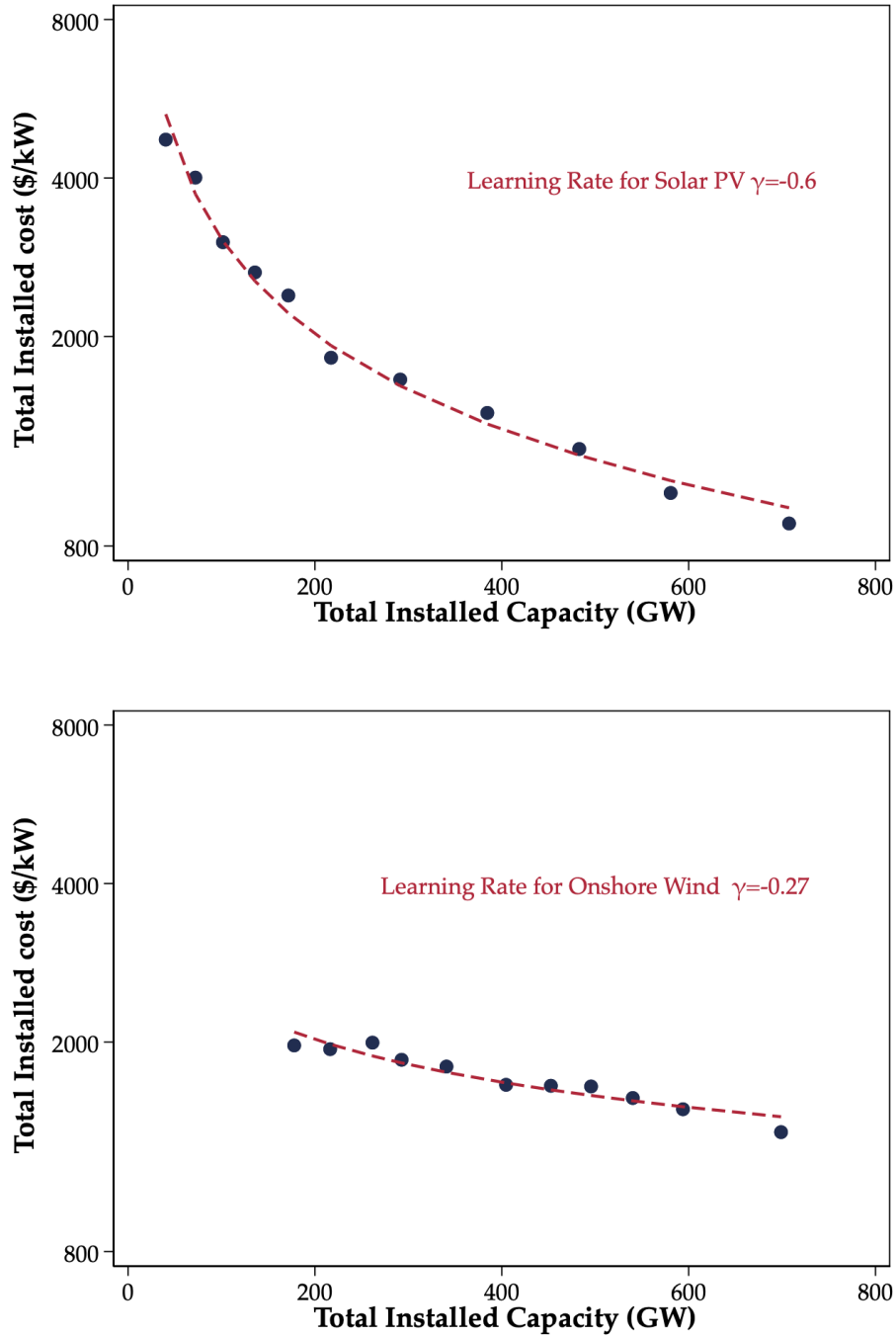
Notes: The left panel plots the share of a country's total electricity usage that comes from wind or solar. The right panel plots the levelized cost of energy from a new solar energy project across countries.Data for the left panel comes from the International Renewable Energy Agency, while the right panel uses data from the BP Statistical Review.

Figure A4: Some Simple Network Examples

(a) Star network   *(b) Ring network*
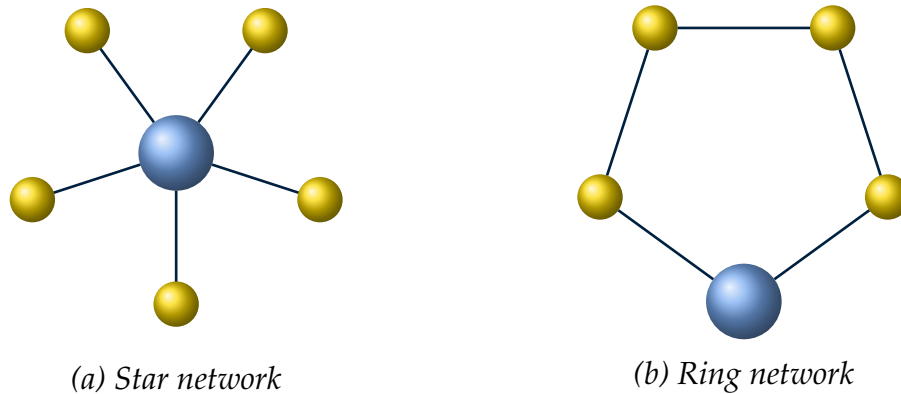
Notes: This figure shows the star and ring network examples discussed in the text, with the swing bus in blue.

A2   Data Construction

In this section we provide details about the construction of data used in the paper. The data consists of two primary components: asset data and grid data.

A2.1   Power Assets

To generate the asset data we use the Global Power Plant (GPP) database, which consists of over 35,000 power plants in 167 countries, each with a name, primary fuel type, geolocation, and power capacity information. We cross-reference the data with official sources from numerous countries to ensure accuracy.[12]

A2.2   Electrical Grid

We use Open Street Map (OSM) data and a Java tool called Osmosis to filter out all non-power-grid data. After filtering we perform further cleaning on the extracted data. We use the power stations and plants in the OSM data extensively in the cleaning process to determine the start and end points of transmission line segments but use the asset data from GPP as this dataset is far richer for assets. The following is a high-level summary of the operations performed by our algorithm.

At any given location, there may be multiple polygons representing different buildings or components within the same "station". We use the term "station" as a catch-all term

---

[12]Our version of the data was downloaded on November 30, 2020.

Figure A5: Spatial Electricity Prices
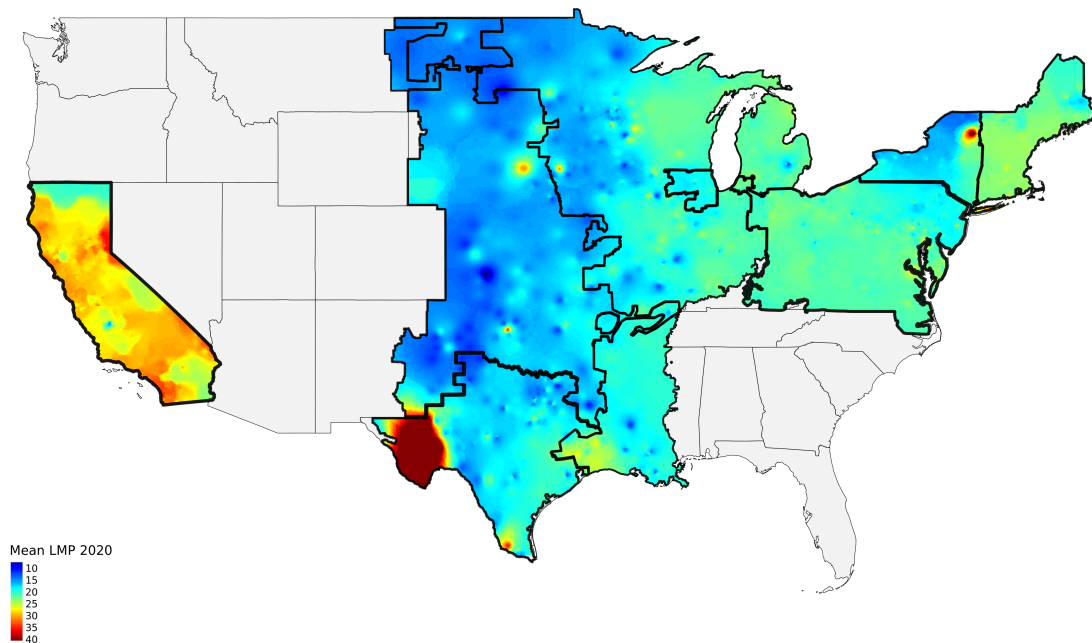
(a) Data
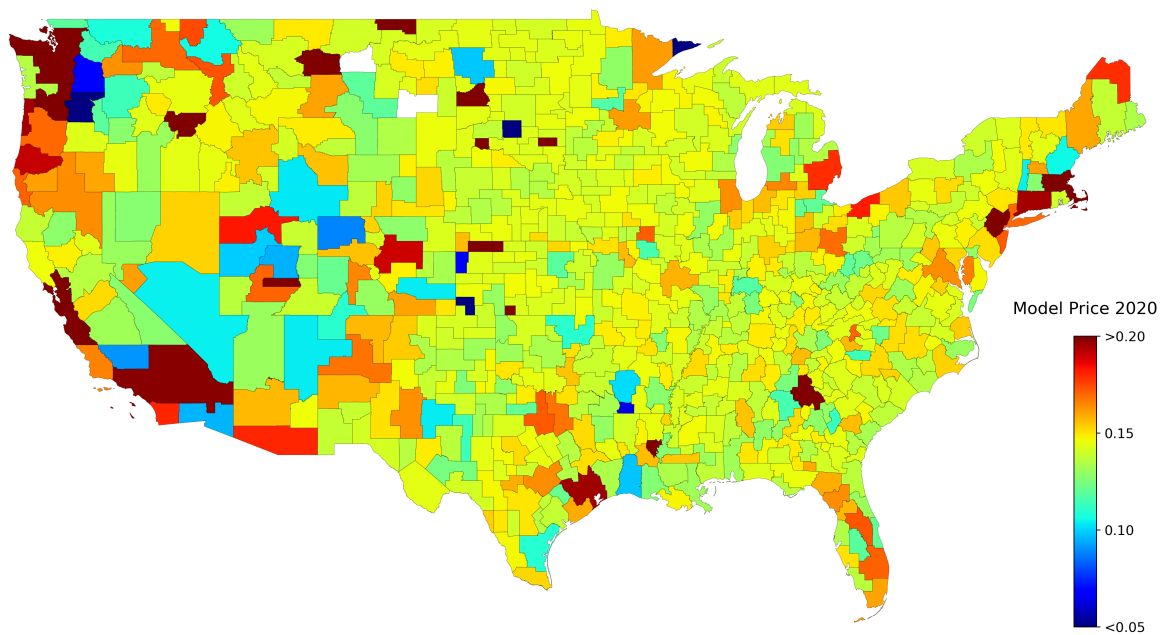
(b) Model

Notes: The top panel of this figures show locational marginal prices from 9 RTO/ISOs in the continental US. Data are average at each pricing noded for 2020, and then smoothed over space. The bottom panel shows the model predictions for prices in 2020 for all US commuting zones.

to describe plants, stations, substations and transformers. As such, we cluster stations within 500 meters of each other.[13]After clustering the stations, we replace line endpoints with the relevant station centroids, either stations intersecting or within 500 meters of the of line, at each step. Spotchecks on Google Earth confirm that many lines that actually connect to nearby stations in reality are not captured by an intersection in the OSM data; instead the lines end outside of the polygon. Incorporating nearby stations addresses this problem. After we complete the line endpoint replacement, lines which are intersected by one or more stations are split.As a result a unique line is defined as one that connects at most two stations. This is also done for stations that are within 500 meters of lines by taking the closest point on the line to the nearby station, buffering it to account for tolerance issues, and subtracting that buffered object from the line. Each line is given a new unique ID number after splitting.

We merge lines together when they have separate IDs and are connected, or within 500 meters of each other, with no station in between. For T-intersections, we take two approaches. A T-intersection is defined as an intersection between two lines A and B where A intersects (or lies within a 500 meter radius of) Line B but not at line B's endpoint. In cases where the relationship is symmetric between A and B, we combine the lines into a single lineWhen the T-intersection is not symmetric (the more common case), the top of the T is split by the bottom, and an artificial station called an "auxiliary" station is constructed at that point to keep track of the intersection. Next, lines which do not intersect any other lines at endpoints are removed and all lines are straightened between their endpoints. . Finally, lines which do not intersect any stations or other lines are dropped.

The post-algorithm grid data and the GPP asset data are both granular because each observation is at the line or station level. As such we aggregate assets and grid lines using the same geographical borders as for our employment and value added data, as in Figure 5. We use each geographical region as a single node located at its centroid and aggregate lines, by counting the number of lines that pass from one geographical area to another, and sum the voltages. The result is a simplified network where any region that has a transmission line into another region is represented by being connected in the network. Using the simplified network, we construct a symmetric adjacency matrix with entries indicating the number of transmission lines from one region to another.

A3   Electrical Line Losses

In this section we derive network losses as a function of power injections and withdrawals int the network. This discussion follows Bohn et al. (1984), where we have

---

[13]This involves grouping stations within 500 meters of one another and taking the convex hull of each group as our final station.

provided additional detail for clarity. We consider lines with resistance R_k and inductance X_k. The impedance magnitude is $z_k = (X_k^2 + R_k^2)^{\frac{1}{2}}$, which is sufficient to know to compute the losses, and we call

$$\Omega_k = z_k^{-1} \tag{A1}$$

the admittance of a line. Let S denote the sending end of the line and R the receiving. Ohm's law for AC circuits gives that the current flowing out of S is equal to

$$I_S = \frac{V_S - V_R}{B_k}$$

where I_S is the current at the sending end of the line, $V_S - V_R$ is the voltage drop across the line k, and B_k is the impedance of the line. These are complex-valued variables, and have an asosociated magnitude and angle, such that

$$I_S = \frac{|V_S|e^{j\delta_S} - |V_R|e^{j\delta_R}}{|z_k|e^{jb}}$$

where δ_S and δ_R are the voltage angles in S and R and b is the angle shift induced by the line itself, and following the notation of the electrical engineering literature, $j = \sqrt{-1}$. Define $\Delta \equiv \delta_S - \delta_R$. The same expression holds for I_R. Apparent power is defined as

$$T_S = Z_S + jQ_S = V_S I_S^*$$
$$T_R = Z_R + jQ_R = V_R I_R^*$$

where Z is real power (the component of power that can do useful work) and Q is reactive power. This can be written in polar form as

$$T_S = \Omega_k |V_S| \left(|V_S|e^{j(b)} - |V_R|e^{j(b-(\delta_R - \delta_S))} \right)$$
$$T_R = \Omega_k |V_R| \left(|V_S|e^{j(b-(\delta_S - \delta_R))} - |V_R|e^{jb} \right)$$

Now assuming that voltages are constant and unitised everywhere ($|V_S| = |V_k| = 1$), we can write real power flows out of S and into R as

$$Z_S = \Omega_k(\cos(b_k) - \cos(b_k + \Delta_k))$$

$$Z_R = \Omega_k(\cos(b_k) - \cos(b_k - \Delta_k))$$

Note that with power flowing from S to R, we have $P_S > 0 > P_R$. Total real power losses on the line are

$$\lambda_k = Z_S + Z_R = \Omega_k 2\cos(b_k) - \Omega_k(\cos(b_k - \Delta_k) + \cos(b_k + \Delta_k))$$

which can be written

$$\lambda_k = \Omega_k 2\cos(b_k) - \Omega_k 2\cos(b_k)\cos(\Delta_k) =$$

$$= \Omega_k 2\cos b_k(1 - \cos(\Delta_k)) \approx \Omega_k 2\left(\cos(b_k)\right)\left(\frac{\Delta_k^2}{2}\right) = R_k \Omega_k^2 \Delta_k^2 \qquad \text{(A2)}$$

where in the second line we have used a second-order approximation to $1 - \cos(\Delta) \approx \Delta^2/2$, assuming that Δ_k is small, and that $b_k = \cos^{-1}(R_k/z_k)$ and the definition in (A1). Note also that

$$Z_k = \Omega_k(\cos(b) - \cos(b + \Delta)) = \Omega_k 2\sin\left(\frac{2b + \Delta_k}{2}\right)\sin\left(\frac{\Delta_k}{2}\right) \approx \Omega_k^2 X_k \Delta_k$$

where we have taken a second order expansion as Δ_k becomes small. Now assuming that $R_k << X_k$, we have $\Omega_k^{-1} = z_k \approx X_k$. So we can write

$$Z_S = \Omega_k \Delta_k \qquad \text{(A3)}$$

and using (A2) we finally arrive at

$$\lambda_k = R_k(Z_S)^2 \qquad \text{(A4)}$$

As above, let $\bar{A}$ be the *bus-branch incidence matrix* of dimension $K \times (N-1)$. Each row consists of a 1, a -1 and zeros. The "direction" of a power-line is arbitrary (i.e. suppose line k has a 1 for node m and -1 for node n in the matrix $\bar{A}$. Then a positive value for Z_k indicates net real power flow from m to n, while a negative value will show power flowing in the other direction). Power injections $P_j = Y_j^{\mathcal{E}} - D_j$ must satisfy

$$P = \bar{A}'Z \qquad \text{(A5)}$$

such that power injected equals the sum of flows out of the bus. The Jth node is called the "swing bus", and power flows there are determined by the energy balance constraint, which can be written

$$e'P + P_J - \lambda = 0$$

where e is a $(J-1)$ vector of ones, and $\lambda = \sum_k \lambda_k$ is total system losses. Now, the incidence matrix $\bar{A}$ allows us to write all the voltage differences Δ on each line as

$$\Delta = \underset{K \times N-1}{\bar{A}} \delta$$

where δ is a $N-1$ vector of voltage phase differences on each node from the swing bus.

Now using equation ([A3](#)), we can write the $K \times 1$ vector of power flows $\boldsymbol{Z}$ as

$$\boldsymbol{Z} = \bar{\boldsymbol{\Omega}}\boldsymbol{\Delta}$$

where $\bar{\boldsymbol{\Omega}}$ is a $K \times K$ diagonal matrix of line admittances with $\Omega_k = (R_k^2 + X_k^2)^{-\frac{1}{2}}$ on the diagonal and 0 on the off-diagonal elements. Combine this with ([A5](#)) to get

$$\boldsymbol{P} = \bar{\boldsymbol{A}}'\bar{\boldsymbol{\Omega}}\bar{\boldsymbol{A}}\boldsymbol{\delta}$$

and use this to get the voltage angles

$$\boldsymbol{\delta} = (\underset{N-1 \times K}{\bar{\boldsymbol{A}}'} \underset{K \times K}{\bar{\boldsymbol{\Omega}}} \underset{K \times N-1}{\bar{\boldsymbol{A}}})^{-1} \underset{N-1 \times 1}{\boldsymbol{P}}$$

in terms of properties of the electricity network.

Finally, the flows on each line are

$$\boldsymbol{Z} = \bar{\boldsymbol{\Omega}}\bar{\boldsymbol{A}}(\bar{\boldsymbol{A}}'\bar{\boldsymbol{\Omega}}\bar{\boldsymbol{A}})^{-1}\boldsymbol{P} \tag{A6}$$

Lastly, let $\bar{\boldsymbol{R}}$ be a diagonal matrix with R_k on the diagonal. Using ([A4](#)), we can write

$$\lambda = \boldsymbol{Z}'\bar{\boldsymbol{R}}\boldsymbol{Z} \tag{A7}$$

A4 Proofs and Additional Results

A4.1 Lemma 1

Proof. With constant resistance-inductance ratio across all lines, we have $\bar{\boldsymbol{R}} = \alpha\bar{\boldsymbol{\Omega}}^{-1}$ for some positive α. Replace $\boldsymbol{Z}$ in ([A7](#)) using ([A6](#)) and obtain

$$\begin{aligned} \lambda &= \left(\bar{\boldsymbol{\Omega}}\bar{\boldsymbol{A}}(\bar{\boldsymbol{A}}'\bar{\boldsymbol{\Omega}}\bar{\boldsymbol{A}})^{-1}\boldsymbol{P}\right)' \alpha\bar{\boldsymbol{\Omega}}^{-1}\bar{\boldsymbol{\Omega}}\bar{\boldsymbol{A}}(\bar{\boldsymbol{A}}'\bar{\boldsymbol{\Omega}}\bar{\boldsymbol{A}})^{-1}\boldsymbol{P} \\ &= \alpha(\bar{\boldsymbol{A}}'\bar{\boldsymbol{\Omega}}\bar{\boldsymbol{A}})^{-1}\bar{\boldsymbol{A}}'\bar{\boldsymbol{\Omega}}\bar{\boldsymbol{A}}(\bar{\boldsymbol{A}}'\bar{\boldsymbol{\Omega}}\bar{\boldsymbol{A}})^{-1}\boldsymbol{P} \\ &= \alpha(\bar{\boldsymbol{A}}'\bar{\boldsymbol{\Omega}}\bar{\boldsymbol{A}})^{-1}\boldsymbol{P} \end{aligned}$$

Define

$$\bar{\boldsymbol{B}} \equiv \alpha(\bar{\boldsymbol{A}}'\bar{\boldsymbol{\Omega}}\bar{\boldsymbol{A}})^{-1} = (\bar{\boldsymbol{A}}'\bar{\boldsymbol{R}}^{-1}\bar{\boldsymbol{A}})^{-1}$$

Now note we can write

$$\bar{\boldsymbol{A}}'\bar{\boldsymbol{R}}^{-1}\bar{\boldsymbol{A}} = \left(\bar{\boldsymbol{R}}^{-\frac{1}{2}}\bar{\boldsymbol{A}}\right)' \bar{\boldsymbol{R}}^{-\frac{1}{2}}\bar{\boldsymbol{A}}$$

A10

since $\bar{R}$ is diagonal. Then since $\bar{A}$ has linearly independent columns by inspection, $\bar{R}^{-\frac{1}{2}}\bar{A}$ has linearly independent columns. Recall that a matrix is positive definite if and only if it can be written as $\bar{X} = \bar{Y}'\bar{Y}$ for some possibly rectangular matrix $\bar{Y}$ with independent columns. Since $\bar{A}'\bar{R}^{-1}\bar{A}$ is positive definite, it is invertible, and its inverse $\bar{B}$ is also positive definite. $\qquad\square$

A4.2 Proposition 1

Proof. Begin by with the problem of the planner who picks quantities $Y_j^{\mathcal{E}}$ and D_j to maximise the sum of consumer and producer surplus. Choose a node b as the reference "swing bus". We can rewrite the planner's problem by substituting in the power balance constraint into the objective function to get

$$\max_{\{P_j\},\{D_j\}} \sum_j p_j Q_j(D_j) - \sum_{j \neq b} M_j(P_j + D_j) - M_b\left(P'\bar{B}P + D_b - \sum_{j \neq b} P_j\right) \tag{A8}$$

subject to

$$0 \leq P_j + D_j \leq \bar{Y}_j^{max} \tag{A9}$$

$$|\bar{\Omega}\bar{A}(\bar{A}'\bar{\Omega}\bar{A})^{-1}P| \leq Z^{max} \tag{A10}$$

Note that $G_j(P, D) = P_j + D_j$ is convex, and $H(P, D) = P'\bar{B}P + D_b - \sum_{j \neq b} P_j$ is convex by the positive definiteness of $\bar{B}$ (see Lemma 1). . Then since M_j and M_b are non-decreasing convex functions, $\sum_{j \neq b} M_j(P_j + D_j) + M_b(P'\bar{B}P - \sum_{j \neq b} P_j + D_b)$ is convex. Hence the planner's objective function maximizes a strictly concave function over a convex set defined by the linear inequality constraints in (A9) and (A10).

Then all that remains to show is that this solution can be implemented by choosing prices appropriately. The FOC's of the original planning problem are

$$p_j Q_j'(D_j) - \sum_k \eta_k \frac{\partial Z_k}{\partial D_j} - \mu\left(1 + \frac{\partial \lambda}{\partial D_j}\right) = 0$$

$$-M_j'(Y_j^{\mathcal{E}}) - \mu_j - \sum_k \eta_k \frac{\partial Z_k}{\partial Y_j} - \mu\left(-1 + \frac{\partial \lambda}{\partial Y_j}\right) = 0$$

where η_k are the Lagrange multipliers on additional line capacity on line k, μ is the multiplier on total system generation and μ_j is the multiplier on extra generating capacity at j. Note that by the definition of P, we have

$$\frac{\partial Z_k}{\partial D_j} = -\frac{\partial Z_k}{\partial Y_j}$$

and

$$\frac{\partial \lambda}{\partial D_j} = -\frac{\partial \lambda}{\partial Y_j}$$

Note that the FOC of final goods producers will satisfy

$$p_j Q'_j(D_j) = p_j^{\mathcal{E},D}$$

and for unconstrained electricity generators we get

$$M'_j(Y_j^{\mathcal{E}}) = p_j^{\mathcal{E},S}$$

So note that setting prices equal to

$$p_j^{\mathcal{E},D} = p_j^{\mathcal{E},S} = \sum_k \eta_k \frac{\partial Z_k}{\partial D_j} + \mu \left(1 + \frac{\partial \lambda}{\partial D_j}\right)$$

at unconstrained generating nodes will induce optimal behaviour. $\square$